



**HAL**  
open science

## Phosphonate-substituted porphyrins as efficient, cost-effective and reusable photocatalysts

Aznar Kechiche, Shaymaa Al Shehimi, Lhoussain Khrouz, Cyrille Monnereau, Christophe Bucher, Stephane Parola, Alla G. Bessmertnykh-Lemeune, Yoann Rousselin, Andrey V. Cheprakov, Habib Nasri

► **To cite this version:**

Aznar Kechiche, Shaymaa Al Shehimi, Lhoussain Khrouz, Cyrille Monnereau, Christophe Bucher, et al.. Phosphonate-substituted porphyrins as efficient, cost-effective and reusable photocatalysts. Dalton Transactions, 2024, 53 (17), pp.7498-7516. 10.1039/D4DT00418C . hal-04797943

**HAL Id: hal-04797943**

**<https://hal.science/hal-04797943v1>**

Submitted on 29 Nov 2024

**HAL** is a multi-disciplinary open access archive for the deposit and dissemination of scientific research documents, whether they are published or not. The documents may come from teaching and research institutions in France or abroad, or from public or private research centers.

L'archive ouverte pluridisciplinaire **HAL**, est destinée au dépôt et à la diffusion de documents scientifiques de niveau recherche, publiés ou non, émanant des établissements d'enseignement et de recherche français ou étrangers, des laboratoires publics ou privés.

# Phosphonate-substituted porphyrins as efficient, cost-effective and reusable photocatalysts

Aznar Kechiche,<sup>a</sup> Shaymaa Al Shehimi,<sup>a</sup> Lhoussain Khrouz,<sup>a</sup> Cyrille Monnereau,<sup>\*,a</sup> Christophe Bucher,<sup>a</sup> Stephane Parola,<sup>a</sup> Alla Bessmertnykh-Lemeune,<sup>\*,a</sup> Yoann Rousselin,<sup>b</sup> Andrey V. Cheprakov,<sup>c</sup> Habib Nasri<sup>d</sup>

<sup>a</sup> ENS de Lyon, UMR 5182, CNRS, Université Claude Bernard Lyon 1, Laboratoire de Chimie, 69342 Lyon, France

<sup>b</sup> Institut de Chimie Moléculaire de l'Université de Bourgogne, UMR CNRS 6302, Université Bourgogne Franche-Comté, 9 Avenue Alain Savary, 21078 Dijon, France

<sup>c</sup> Lomonosov Moscow State University, Department of Chemistry, 1-3, Leninskie Gory, Moscow, 119991, Russia

<sup>d</sup> University of Monastir, Laboratory of Physical Chemistry of Materials (LR01ES19), Faculty of Sciences of Monastir, Avenue of the environment, 5019 Monastir, Tunisia

## Abstract

Recent advances in visible light photocatalysis represent a significant stride towards sustainable catalytic chemistry. However, their successful implementation in fine chemical production remains challenging and requires careful optimization of available photocatalysts. Our work aims to structurally modify bioinspired porphyrin catalysts, addressing issues related to their laborious synthesis and low solubility, with the goal of increasing their efficiency and developing reusable catalytic systems. We have demonstrated the catalytic potential of readily available *meso*-tetrakis[4-(diethoxyphosphoryl)phenyl]porphyrins (M(TPPP)). Novel metal (Pd(II), Co(II) and In(III)) complexes with this ligand were prepared in good yields. These chromophores were characterized in solution using spectroscopic (NMR, UV-vis, fluorescence) and electrochemical methods. The introduction of phosphonate groups on the phenyl substituents of *meso*-tetraphenylporphyrins (M(TPP)) improves solubility in polar organic solvents without significantly altering the photophysical properties and photostability of complexes. This structural modification also leads to easier reductions and harder oxidations of the macrocycle for all investigated complexes compared to corresponding TPP derivatives. The free base porphyrin, zinc(II), palladium(II), and indium(III) complexes were studied as photocatalysts for oxidation of sulfide to sulfoxides using molecular oxygen as a terminal oxidant. Both dialkyl and alkyl aryl sulfides were quantitatively transformed into sulfoxides under blue LED irradiation in the acetonitrile–water mixture (10:1 v/v) with a low loading (0.005–0.05 mol%) of porphyrin photocatalysts, where H<sub>2</sub>(TPPP) and Pd(TPPP) were found to be the most efficient. The reaction mechanism was studied using photoluminescence and EPR

spectroscopies. Then, to access reusable catalysts, water-soluble derivatives bearing phosphonic acid groups,  $H_2(TPPP-A)$  and  $Pd(TPPP-A)$ , were prepared in high yields. These compounds were characterized using spectroscopic methods. Single-crystal X-ray diffraction analysis of  $Pd(TPPP-A)$  reveals that the complex forms a 3D hydrogen-bonded organic framework (HOF) in the solid state. Both  $H_2(TPPP-A)$  and  $Pd(TPPP-A)$  were found to catalyzed the photooxidation of sulfides by molecular oxygen in acetonitrile–water mixture (MeCN– $H_2O$ , 1:1 v/v), while only  $Pd(TPPP-A)$  resulted in selective production of sulfoxides. The complex  $Pd(TPPP-A)$  was easily recovered through extraction in aqueous phase and successfully reused in five consecutive cycles of the sulfoxidation reaction.

## INTRODUCTION

Over the past two decades, there has been a remarkable increase in the utilization of photocatalysis in organic synthesis.<sup>1,2</sup> This surge can be primarily attributed to the demand for sustainable processes and the rapid development of photoredox catalytic reactions that operate through one-electron transfer pathways.<sup>3-4</sup> Photoredox processes have greatly expanded the range of available synthetic tools to obtain complicated organic molecules under mild conditions, allowing for potential use of renewable energy source (sunlight). Photocatalysis is also important for optimizing hazardous or expensive processes such as oxidation and cross-coupling reactions, for instance. Nevertheless, several notable drawbacks must be still addressed to make these reactions truly suitable for achieving the ultimate objectives of sustainable chemistry.

First, many of photocatalytic processes require the use of scavengers or sacrificial reagents, most often organic compounds, producing many side products in the reaction mixture that make purification of the target products difficult. Additionally, the most commonly employed photocatalysts are expensive Ru(II) and Ir(III) complexes.<sup>7,8</sup> The substitution of these catalysts with organic dyes has been extensively investigated; however, high loading levels of these photocatalysts are often necessary due to the low photostability of organic dyes. By-products generated during photodecomposition of these catalysts must also be separated from the target products. Furthermore, the choice of solvents for photocatalytic processes is often limited, posing a challenge for the development of industrial-scale processes in which many organic solvents are prohibited by regulatory norms. The last but not the least, the efficiency of light utilization in these processes remains rather low.

To address these challenges, optimization of available photocatalysts has emerged as a crucial objective.<sup>9-11</sup> This would enable shorter irradiation times, reduced photocatalyst loading, and the use of more environmentally friendly solvents. Porphyrin derivatives, renowned for their remarkable photophysical properties and prevalence in natural catalytic processes, were identified early on as promising compounds.<sup>12-14</sup> However, the synthetic availability and limited solubility of these compounds present significant challenges. Porphyrins are usually only soluble in chlorinated solvents, which are toxic and can participate in radical processes in particular in the presence of oxygen and catalysts.<sup>15-17</sup> This leads to decreased reaction selectivity and accelerated photocatalyst decomposition.

Another crucial aspect in the development of porphyrin photocatalysts is our knowledge of the superior catalytic activity exhibited by derivatives bearing perfluorinated or sterically hindered *ortho*-disubstituted aryl groups in the *meso*-positions of the macrocycle (so-called second generation catalysts).<sup>18-20</sup> Nevertheless, the synthesis of these derivatives is generally more difficult compared to the classical *meso*-tetraphenylporphyrins (M(TPP)), and this significantly limits their overall advantages. It is worth to emphasize that the superiority of these photocatalysts, when compared to TPP complexes, has been primarily demonstrated in oxidation processes involving strong oxidants. Their significance may be less pronounced in photoredox transformations and other photocatalytic processes proceeding under mild reaction conditions.

In this context, we hypothesized that 5,10,15,20-tetra[4-(diethoxyphosphoryl)phenyl]porphyrins H<sub>2</sub>(TPPP) and its metal complexes (Fig. 1) could be promising as photocatalysts. Electron-deficient H<sub>2</sub>(TPPP) indeed exhibits a good solubility in various organic solvents, and the diethoxyphosphoryl substituents can serve as anchoring groups for heterogenization of photocatalysts through grafting onto titania or zirconia supports or through preparation of metal-organic frameworks (MOFs).<sup>21-23</sup> Furthermore, these porphyrins can be easily transformed into water-soluble derivatives through hydrolysis of the phosphonate diester groups.<sup>24</sup> In catalytic processes, these water-soluble compounds could be easily separated from the target organic products through liquid phase extraction.<sup>25</sup>

In this work, we synthesized Pd(II), In(III), and Co(II) complexes of H<sub>2</sub>(TPPP) (Fig. 1) and thoroughly investigated their redox and photophysical properties. Their utility in the photooxidation of sulfide to sulfoxides using molecular oxygen as the terminal oxidant was also explored. We developed a practical experimental procedure for selective sulfoxidation in non-chlorinated solvents, with either the free base porphyrin H<sub>2</sub>(TPPP) or the Pd(II) complex

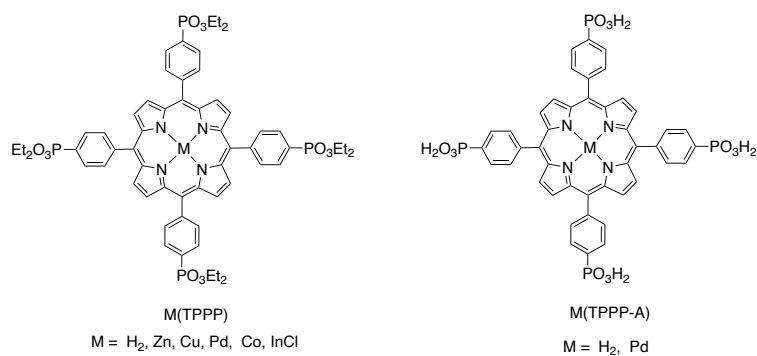


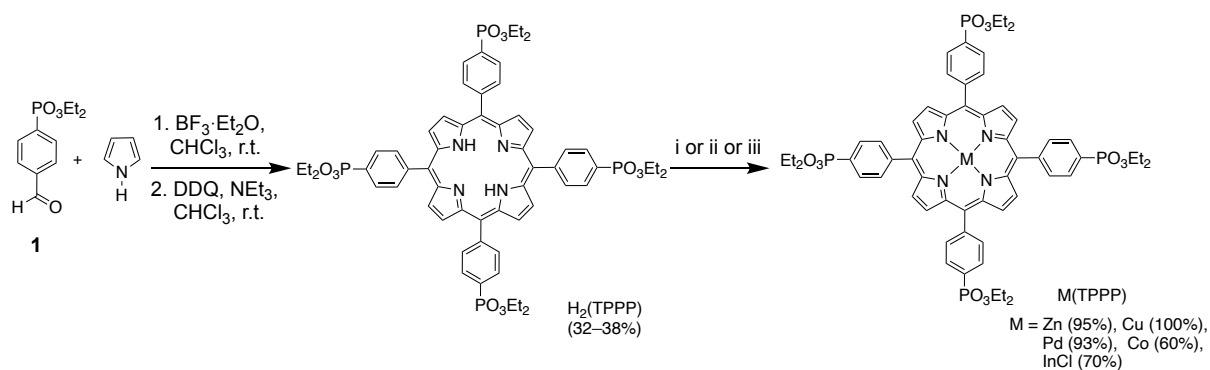
**Fig. 1.** Phosphonate-substituted porphyrins investigated in this work.

serving as a photocatalyst. Furthermore, we successfully prepared water-soluble derivatives H<sub>2</sub>(TPPP-A) and Pd(TPPP-A) (Fig. 1) and demonstrated that Pd(TPPP-A) is an efficient photocatalyst for sulfoxidation reaction and can be easily recovered by extraction in the aqueous phase and reused in subsequent catalytic cycles.

## RESULTS AND DISCUSSION

### Synthesis of photocatalysts

The free-base porphyrin H<sub>2</sub>(TPPP) and their complexes have been extensively used in material chemistry and sensing,<sup>26–29</sup> and their synthesis has been meticulously optimized (see the ESI† for the additional details). In this work this compound was prepared by the introduction of the diethoxyphosphoryl group in the aldehyde molecule following the classical condensation of pyrrole and diethyl (4-formylphenyl)phosphonate (**1**) under acidic conditions (Scheme 1).



<sup>a</sup> Reagents and conditions: (i) M(OAc)<sub>2</sub> (M = Zn, Cu, Co), CHCl<sub>3</sub>/MeOH, reflux; (ii) Pd(OAc)<sub>2</sub>, CHCl<sub>3</sub>/MeCN, reflux; (iii) InCl<sub>3</sub>, AcOH, NaOAc, reflux.

**Scheme 1.** Synthesis of M(TPPP) porphyrins.

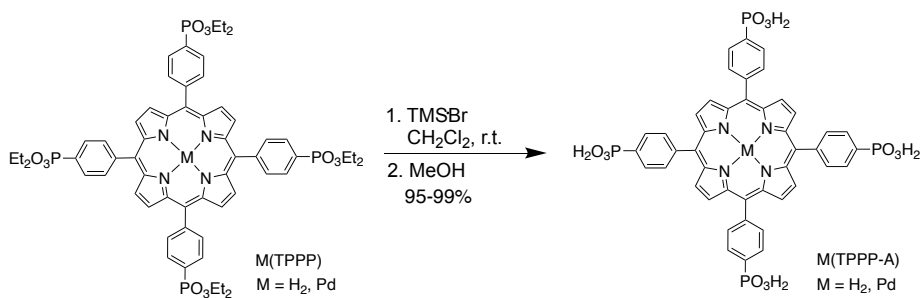
Due to the electron-deficient character of  $H_2(TPPP)$  and its good solubility in common organic solvents, the insertion of various metal ions into this macrocycle proceeds under mild conditions. The synthesis of complexes with redox-inactive metals such as Zn(II), Cu(II), and Ni(II) has already been reported.<sup>30,31</sup> In this work, we prepared Pd(II), Co(II), and In(III) complexes, which are of interest for catalytic applications (Scheme 1). Pd(II) and Co(II) complexes were obtained by adding an excess of metal acetate salts to solutions of  $H_2(TPPP)$  in a refluxed  $CHCl_3/MeCN$  and  $CHCl_3/MeOH$  solvent mixture, respectively. The palladium complex could be obtained in 95% yield by ensuring that heating was stopped immediately after the consumption of the starting compound. The Co(II) complex was obtained in only 60% yield, even when stopping the reaction immediately after the complete consumption of  $H_2(TPPP)$ . For the insertion of In(III) ions, indium(III) chloride was used as a metal source, and the reaction was conducted in refluxed acetic acid in the presence of sodium acetate as a buffer. The target complex was obtained in 70% yield.

We also attempted to prepare Cr(III) complex Cr(TPPP) by reacting  $H_2(TPPP)$  with chromium(II) dichloride or chromium(0) hexacarbonyl, following the procedures reported for the preparation of chromium(III) complexes of  $H_2(TPP)$ .<sup>32,33</sup> However, the target compound could not be isolated likely due to the hydrolysis of the diethyl phosphonate substituents in the presence of Cr(III) ions, known for their strong Lewis acid properties.

Next, we prepared water-soluble porphyrins  $H_2(TPPP-A)$  and Pd(TPPP-A) bearing four phosphonic acid substituents. Carrying out the reaction  $H_2(TPPP)$  with an excess of concentrated HCl in a refluxing mixture of MeOH/THF for 48 h led to a complex mixture of partially hydrolyzed porphyrins. The target compound  $H_2(TPPP-A)$  was obtained reacting  $H_2(TPPP)$  with an excess of TMSBr in  $CH_2Cl_2$  following by the treatment with methanol (Scheme 2). These conditions were also found to be suitable for achieving a high yield in the synthesis of Pd(TPPP-A).

It is worth mentioning that an alternative method, involving the insertion of Pd(II) ions into  $H_2(TPPP-A)$ , was reported after the completion our synthetic work.<sup>34</sup>

The structures of synthesized porphyrins M(TPPP) and M(TPPP-A) were confirmed by HRMS, NMR, and FT-IR analyses (Fig. S29–S52, ESI<sup>†</sup>) and by single crystal X-ray diffraction analysis of Pd(TPPP-A) (see below). All synthesized M(TPPP) complexes were found to be soluble in chlorinated organic solvents, MeOH, MeCN, THF, and DMF (at the level up to mM).



**Scheme 2.** Synthesis of phosphonate-substituted porphyrins M(TPPP-A).

DFT computations of selected M(TPPP) (M = H<sub>2</sub>, Pd, InCl) were performed using a B3LYP functional and the Jorge-DZP basis set for all atoms. The calculations were simplified by replacing ethyl substituents of phosphonate groups by methyl groups and corresponding compounds were labeled M(TPPP-Me). According to these calculations, all molecules contain a planar porphyrin core, with the phenyl rings turned out of plane by angles that are sufficiently

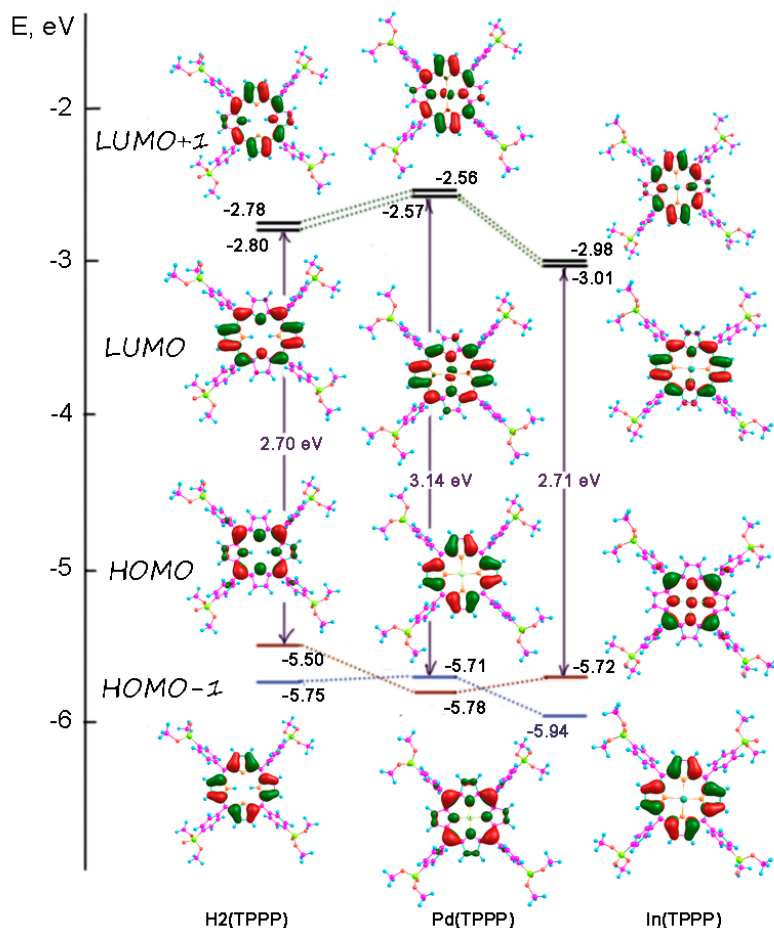


**Fig. 2.** The isodensity plot of HOMO and LUMO orbitals for model chromophores M(TPPP-Me) (M = H<sub>2</sub>, Pd, InCl) obtained from DFT calculations.

large for minimizing conjugation between the core and the rings (Fig. S26-28<sup>†</sup> and Table S7<sup>†</sup>). All orbitals of the frontier bundle are typical for the generic porphyrin system, as described in the four-orbital Gouterman model (Fig. 2). Thus, redox and photophysical properties are expected to be like those of TPP derivatives. These properties have been studied in detail (see below) to provide all the necessary information for the understanding and analysis of targeted photocatalytic experiments.

### Solid-state structure of Pd(TPPP-A)

Single crystals of Pd(TPPP-A) were grown by slow evaporation a solution of this compound in DMF/water solvent mixture (10:1 v/v). The complex crystallized as solvate and the solvent molecules are numerous and highly disordered in the crystal. An appropriate SQUEEZE procedure was used to obtain crystallographic data (see Experimental data) and their summary is presented in Fig. 3–5, S1–S3<sup>†</sup> and Tables S1–S5<sup>†</sup>).

The complex crystallized in the triclinic *P*-1 space group as a salt with dimethylammonium counter cations (Table S1<sup>†</sup>). The latter species ( $\text{Me}_2\text{NH}_2^+$ ) is probably formed during crystallization of Pd(TPPP-A) due to a slow hydrolysis of DMF under acidic conditions. This side-reaction is commonly observed in solvothermal syntheses of MOF in DMF or DMF/water mixtures.

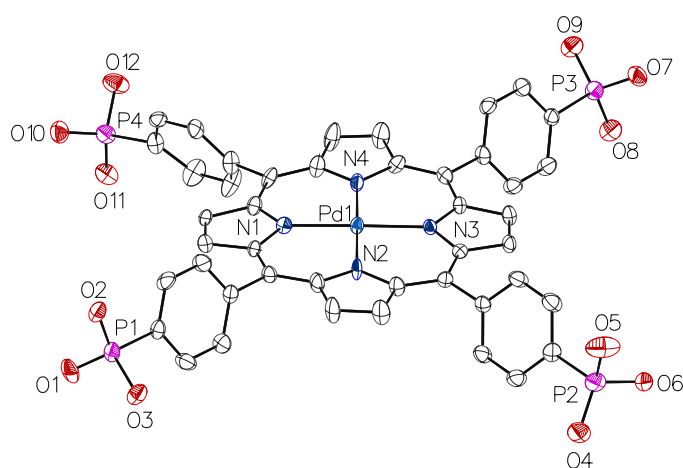


**Fig. 3.** Molecular structure of the complex  $(\text{Me}_2\text{NH}_2)_2[\text{Pd}(\text{TPPP-A})_{-2\text{H}}]$  obtained by single-crystal X-ray analysis. Hydrogen atoms, minor disordered parts and counterions are omitted for clarity.

The asymmetric unit of the crystal contains one porphyrinate molecule and two dimethylammonium cations. The palladium(II) ion adopts a square-planar coordination environment (RMSD plane = 0.006 Å) formed by four nitrogen atoms of the porphyrin



macrocycle (Pd–N = 2.018–2.032 Å, Table S2<sup>†</sup>). The Pd–N bond lengths are consistent with those found in other palladium(II) complexes with porphyrin ligands.<sup>34–37</sup> The displacement of the palladium atom from the N4 mean plane of the macrocycle is within 0.011 Å. The porphyrin macrocycle is flat and the angle between the planes defined by Pd–N(1)–N(2) and Pd–N(3)–N(4) is 1.1(2)° (Table S3<sup>†</sup>). The maximum deviation of the  $\beta$ -carbon atoms from the N4 mean plane does not exceed 0.160 Å, while the deviations of the *meso*-carbon atoms are less than 0.1 Å. The phenyl substituents at the *meso*- positions of the macrocycle exhibit different twist angles with respect to the N4 plane. This is attributed to hydrogen bonding of phosphonate groups and steric interactions between the phenyl rings and pyrrole fragments of adjacent porphyrin molecules (Fig. 3 and 4). The values of these twist angles range from 58.5(2)° to 66.6(3)° (Table S3<sup>†</sup>), which is significantly smaller than 80° observed in Pd(TPP).<sup>35</sup> This observation suggests a significant influence of the phosphonate group on the crystal organization. Phosphonic acids are well-known to form strong hydrogen bonds<sup>38,39</sup> and to promote the formation of networks through this charge-assisted hydrogen bonding.<sup>40,41</sup> In the studied structure, each phosphonate substituent is involved in the formation of two or three hydrogen bonds with phosphonate groups of nearby porphyrin molecules and dimethylammonium cations (Fig. 4). The P–O bond lengths differ significantly in the P=O and P–OH residues, with values lying in the range of 1.499–1.505 Å and 1.549–1.694 Å, respectively (Table S2<sup>†</sup>). The remaining four P–O bonds are very similar, measuring 1.529(4), 1.519(4), 1.519(4), and 1.512(4) Å. The positioning of the two remaining protons can likely be determined by considering that only two adjacent phosphonates form hydrogen bonds with dimethylammonium ions (Fig. 4). The other two phosphonate groups are involved in hydrogen bonding only with phosphonate residues belonging to the neighboring macrocycles, and these phosphonate groups are likely doubly protonated. As illustrated in Fig. 4, S2 and S3<sup>†</sup>, the interaction between the hydrophilic and hydrophobic regions of the molecules is optimized in the crystals and a 3D hydrogen-bonded organic framework (HOF) is formed. In this network, porphyrin macrocycles are organized in chains along the [100] crystallographic direction and are separated by hydrophilic regions. This crystal organization results in the formation of 1D open channels (Fig. 5 and S1<sup>†</sup>).

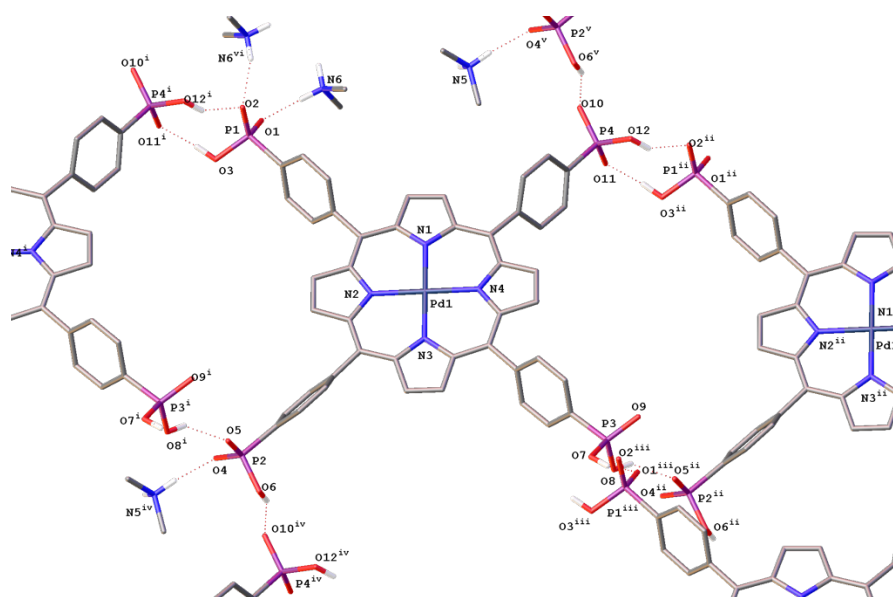


**Fig. 4.** Schematic presentation of HOF formed in the crystal  $(\text{Me}_2\text{NH}_2)_2[\text{Pd}(\text{TPPP-A})\cdot 2\text{H}]$ .

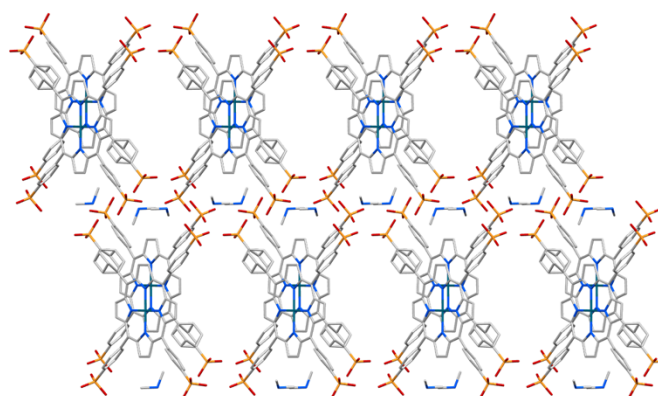


**Fig. 5.** Cation-assisted hydrogen-bonding in the crystals  $(\text{Me}_2\text{NH}_2)_2[\text{Pd}(\text{TPPP-A})\cdot 2\text{H}]$  leading to formation of HOF (view along  $[101]$  crystallographic direction).

The free volume, calculated using the Mercury program,<sup>42</sup> for compositions without solvate molecules in the voids of  $(\text{Me}_2\text{NH}_2)_2[\text{Pd}(\text{TPPP-A})\cdot 2\text{H}]$ , is 25.3% (probe radius 1.2 Å, Fig. S1<sup>†</sup>). This value is approximately twice as high as that observed in the reported complex  $\text{Ni}(\text{TPPP-A})$ , which was crystallized as salts containing 3.5 and 4 dimethylammonium molecules.<sup>43</sup> It is worth noting that networks sustained by inter-porphyrin hydrogen bonds, which have been extensively studied in the past,<sup>44</sup> have recently gained renewed interest as microporous solids.<sup>34,45,46</sup> Our HOF hold potential for the development of photocatalysts and conductive materials. However, these topics are outside the scope of our article.

## Electrochemical properties

The properties of the free base porphyrin H<sub>2</sub>(TPPP) and the complexes formed with Zn(II), Cu(II), Pd(II), Co(III), and In(III) ions were further investigated using cyclic voltammetry (CV), mainly to assess the impact of the metal ions on the redox potentials and on the stability of the oxidized/reduced species.

**Table 1.** Electrochemical data (half-wave potentials or peak potentials in volts vs.  $E_{ref}[Ag^+(0.01M)/Ag]$ ) of the investigated tetra(diethoxyphosphoryl)-substituted porphyrins and referenced compounds in MeCN, dichloromethane (CH<sub>2</sub>Cl<sub>2</sub>) or benzonitrile (PhCN). In this work, cyclic voltammetry measurements were carried out at a vitreous carbon working electrode ( $\varnothing = 3\text{mm}$ ,  $\nu = 0.1\text{ V/s}$ ) in MeCN containing tetra-*n*-butylammonium perchlorate (TBAP, 0.1 M).

Compound	Solvent	Oxidation potentials			Reduction potentials (V) <sup>a</sup>			$E_{1a} - E_{1c}$ (V)	$E_{2a} - E_{1a}$ (V)	$E_{1c} - E_{2c}$ (V)	Ref
		(V) <sup>a</sup>									
		$E_{3a}$	$E_{2a}$	$E_{1a}$	$E_{1c}$	$E_{2c}$	$E_{3c}$				
H <sub>2</sub> (TPPP)	MeCN	1.22 <sup>b</sup>	0.97 <sup>b</sup>	0.81 (71)	-1.35 (62)	-1.72 (65)	-2.39 <sup>b</sup>	2.16	0.16	0.37	tw <sup>c</sup>
H <sub>2</sub> (TPPP)	CH <sub>2</sub> Cl <sub>2</sub>		1.05	0.88	-1.38	-1.68		2.26	0.17	0.30	30
H <sub>2</sub> (TPP)	PhCN		1.03	0.75	-1.45	-1.84		2.20	0.28	0.39	47, 48
Cu(TPPP)	MeCN		0.95 (73)	0.75 (67)	-1.45 (65)	-1.88 (78)		2.20	0.20	0.43	tw
Cu(TPP)	PhCN		1.03	0.69	-1.58	-2.04		2.27	0.34	0.46	49, 48
Zn(TPPP)	MeCN	1.17 <sup>b</sup>	0.78 (96)	0.57 (66)	-1.58 (63)	-1.96 <sup>b</sup>		2.15	0.21	0.38	tw
Zn(TPPP)	CH <sub>2</sub> Cl <sub>2</sub>		0.90	0.60	-1.53	-1.88 <sup>b</sup>		2.13	0.30	0.35	47, 48
Zn(TPP)	PhCN		0.88	0.53	-1.66	-2.02 <sup>b</sup>		2.19	0.35	2.19	47, 48
Pd(TPPP)	MeCN		1.21 <sup>c</sup>	0.93 <sup>c</sup>	-1.44 (64)	-1.89 (66)	-2.35 (104)	2.37	0.28	0.45	tw
Pd(TPP)	PhCN		1.23	0.85	-1.55	-2.05		2.4	0.38	0.5	48
Co(TPPP)	MeCN	1.07 (63)	0.85 (66)	0.22 <sup>b</sup>	-1.08 (71)	-2.13 (80)		na	0.23	1.05	tw
Co(TPP)	PhCN	1.07	0.89	0.28 <sup>b</sup>	-1.15	-2.27		na			50
In(TPPP)	MeCN		1.20 <sup>b</sup>	0.97 <sup>b</sup>	-1.17 (65)	-1.57 (61)	-2.43	2.14	0.23	0.40	tw
In(TPP)	PhCN		1.25 <sup>b</sup>	0.91	-1.39	-1.78		2.30	0.34	0.39	51

<sup>a</sup> Unless noted otherwise, the oxidation and reduction potentials reported in the table are half-wave potential values ( $E_{1/2}$ ); the associated peak to peak potential shifts are given in parenthesis ( $\Delta E_p = |E_{pa} - E_{pc}|$  given in mV). <sup>b</sup> Peak potential value ( $E_{pa}$  or  $E_{pc}$  in V) measured at a scan rate of 0.1 V/min. The following conversion<sup>52</sup> was used to compare potential values (in V) measured versus SCE<sup>30</sup> and  $\text{Ag}^+$  ( $10^{-2}$  M in MeCN + 0.1 M TBAP)/Ag (this work) :  $E_{\text{ref}}(\text{Ag}^+/\text{Ag}) = E_{\text{ref}}(\text{SCE}) + 0.3$ . <sup>c</sup> tw = this work.

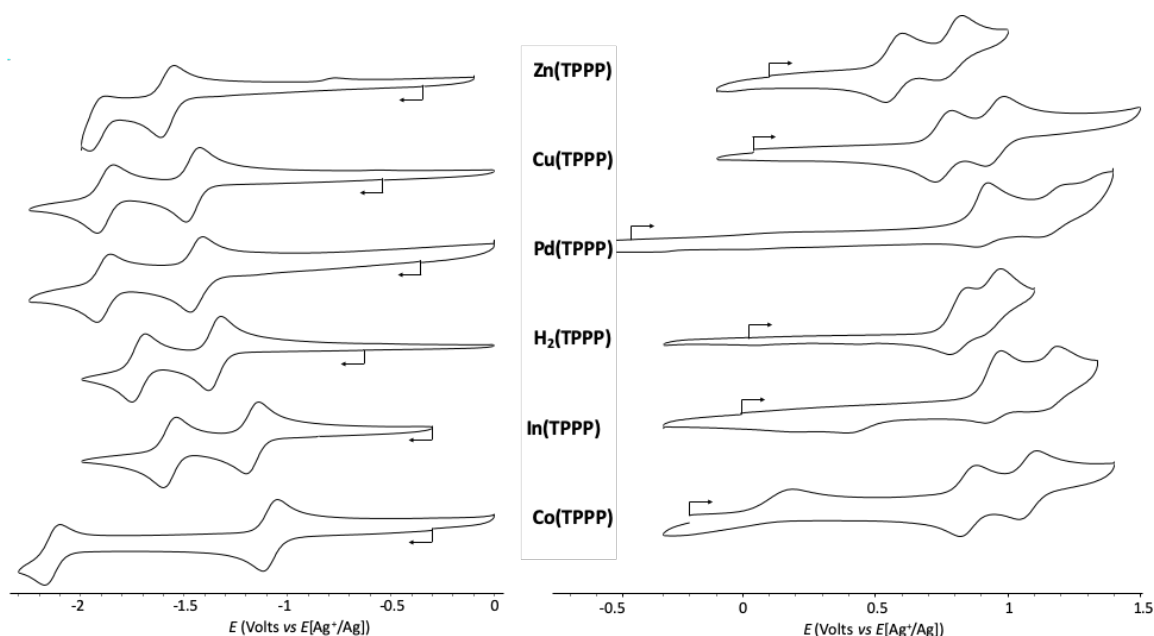


**Fig. 6.** Cyclic voltammograms recorded for  $\text{M}(\text{TPPP})$  with  $\text{M} = \text{Zn}(\text{II}), \text{Cu}(\text{II}), \text{Pd}(\text{II}), \text{H}_2, \text{In}(\text{III})$  and  $\text{Co}(\text{II})$  (1mM in MeCN + TBAP (0.1 M)), vitreous carbon working electrode ( $\varnothing = 3$  mm),  $\nu = 0.1 \text{ V s}^{-1}$ ,  $E$  vs  $[\text{Ag}^+(0.01\text{M})/\text{Ag}]$ .

These experiments were conducted in MeCN containing tetra-*n*-butylammonium perchlorate (TBAP) used as a supporting electrolyte. All relevant data are collated in Table 1 together with those of reference compounds based on *meso*-tetraphenylporphyrin  $\text{M}(\text{TPP})$  and on previously described  $\text{M}(\text{TPPP})$  complexes.<sup>30,31</sup> Selected voltammograms are shown in Fig. 6.

As reported earlier,<sup>30</sup> the free base porphyrin  $\text{H}_2(\text{TPPP})$  undergoes two ring-centered oxidations and two ring-centered reductions, eventually followed by additional fully irreversible waves observed below  $-2$  V or above  $+1$  V (Fig. S4<sup>†</sup>). The electron-withdrawing effect of the four phosphorylated substituents is easily brought to light by the significant anodic shift of all waves compared to those recorded under similar conditions with the reference free base  $\text{H}_2(\text{TPP})$  (Table 1). Only the second oxidation wave at  $E_{\text{pa}2} = 1.21$  V was found to exhibit irreversible character under these experimental conditions as previously observed in dichloromethane.<sup>30,53–55</sup>

The CV curves recorded with the metal complexes M(TPPP) (M = Zn(II), Cu(II), Pd(II), In(III), and Co(II)) are shown in Fig. 6 and S5–S13<sup>†</sup>. These curves bring to light that the nature of the metal ion has a significant impact on the oxidation and reduction potential values.<sup>56,57</sup> Among the investigated compounds, only Cu(TPPP) exhibits two reversible one-electron oxidation waves and two reversible one-electron reduction waves with characteristic absolute potential shifts ( $E_{1a} - E_{1c}$  and  $E_{2c} - E_{1c}$ )<sup>58</sup> demonstrating the successive formation of stable porphyrin-centered  $\pi$ -anion radical and dianion on the cathodic side, and of  $\pi$ -cation radical and dication on the anodic side (Fig. S5<sup>†</sup>).

The replacement of copper(II) with a more electropositive zinc(II) ion has a notable effect on the effective charge density at the macrocycle, leading to a cathodic shift of about 100 mV of both reversible reduction waves. Another notable difference with the data collected with Cu(TPPP) is the more or less significant loss in the reversibility of the second reduction and oxidation waves ( $E_{2a}$  and  $E_{2c}$  in Table 1), the existence of chemical steps associated to the formation of  $[\text{Zn(TPPP)}]^{2+}$  and  $[\text{Zn(TPPP)}]^{2-}$  being further revealed by the observation of a third oxidation wave at  $E_{\text{pa}3} = 1.17$  V of the former ( $[\text{Zn(TPPP)}]^{2+}$ ), and of a weak re-oxidation peak at  $E_p = -0.75$  V of the latter ( $[\text{Zn(TPPP)}]^{2-}$ ) (see Fig. 6 and S6<sup>†</sup>). Such finding is reminiscent of previous studies<sup>59,60</sup> showing that electrogenerated porphyrin dianion can be involved in proton abstraction reactions with the solvent to afford phlorin dianions.

The CV of Pd(TPPP) exhibits one fully irreversible oxidation wave at  $E_{\text{pa}1} = 0.93$  V and three consecutive reduction waves (Fig. 6 and S7<sup>†</sup>). The stability of the anion radical state  $[\text{Pd(TPPP)}]^{•-}$ , initially revealed at the CV time scale by the reversibility of the first reduction wave centered at  $[E_{1/2}]_{1c} = -1.44$  V, was confirmed at the electrolysis time scale by the unambiguous identification of the one-electron reduced species generated *in situ* after exhaustive electrolysis at  $-1.6$  V (Fig. S8<sup>†</sup>), the most notable changes observed on the UV–vis absorption spectra collected over time during this experiment being a large decrease in the intensity of the initial Soret band, coming along with a 25 nm bathochromic shift, and the development of a weakly intense band in the near IR region at  $\lambda_{\text{max}} = 878$  nm. The doubly reduced species  $[\text{Pd(TPPP)}]^{2-}$ , generated by exhaustive reduction of the mixture at  $-2.15$  V, was conversely found to be unstable in our conditions, as revealed by our failure to regenerate Pd(TPPP) by re-oxidation (Fig. S9<sup>†</sup>). As mentioned for the Zn(II) complex, the low stability of the electrogenerated dianion  $[\text{Pd(TPPP)}]^{2-}$  could be explained by its reaction with the solvent to give a phlorin derivative, whose formation under electrolysis conditions ( $E_{\text{app}} = -2.15$  V, Fig. S10<sup>†</sup>) was validated by a red shift of the Soret band (17 nm) and by the development of a broad

absorption band at 785 nm.<sup>48,59,60</sup> The irreversibility of the oxidation wave at  $E_{pa1} = 0.93$  V also contrasts with the Nernstian response observed in similar conditions with parent complexes.<sup>48,61</sup> The absence of a return reduction signal at 100 mV/s (Fig. S10<sup>†</sup>) led us to attribute the irreversibility of the [Pd(TPPP)]<sup>•+</sup>/Pd(TPPP) wave to the poor stability of the cation radical state in our experimental conditions.

The CV curves recorded for the indium(III) complex In(TPPP) exhibit a similar pattern with two consecutive irreversible one-electron oxidation and three reversible reduction waves (Fig. 6, S11 and S12<sup>†</sup>). The irreversibility of the first oxidation wave is attributed to the existence of a coupled chemical reaction. The 400 mV shift measured between the first and second half-wave reduction potentials is in good agreement with values reported in literature for reduction processes centered on the porphyrin ring, which supports the conclusion that the stable complexes [In(TPPP)]<sup>•-</sup> and [In(TPPP)]<sup>2-</sup> are successively produced at the interface. The HOMO–LUMO gap of 1.14 V measured between the first oxidation and reduction waves is also consistent with the *in-situ* formation of the porphyrin-centered anion and cation radicals In(TPPP)<sup>•-</sup> and [In(TPPP)]<sup>•+</sup>, respectively. These values are also in good agreement with those previously reported for similar In(TPP) complexes.<sup>51</sup>

The major discrepancies observed between the curves collected with the cobalt porphyrin Co(TPPP) and those discussed above are attributed to the known electro-activity of the cobalt center which can potentially be oxidized or reduced in the accessible potential range.<sup>48</sup> As previously observed for related complexes,<sup>48,50</sup> three successive one-electron oxidation waves are observed in the anodic domain, including one irreversible wave at  $E_p = 0.22$  V and two irreversible ones at  $E_{1/2} = 0.85$  and 1.07 V (Fig. 6 and S13<sup>†</sup>). The unusual shape and position of the first one-electron oxidation wave allows its unambiguous attribution to the formation of a Co(III) center, while the two subsequent one-electron reversible waves are attributed to porphyrin-centered processes yielding successively a Co(III)  $\pi$ -cation radical and a dication.

On the cathodic side, two reversible one-electron reduction waves are observed at  $E_{1/2} = -1.08$  and  $-2.13$  V ( $E_{1c}$  and  $E_{2c}$  in Table 1). The difference of more than 1 V measured between those two values, *i.e.* more than double those obtained under the same experimental conditions with related M(TPP) complexes (M is non-electroactive metal ion), supports the well-accepted idea<sup>50,56,62–64</sup> that the first one electron reduction is transferred on the Co(II) center and the second one on the organic ligand. These data are thus in agreement with a first

reduction yielding  $[\text{Co(I)(TPPP)}]^-$ , which is then converted at much lower cathodic potentials into the porphyrin anion radical  $[\text{Co(I)(TPPP)}^\bullet]^{2-}$ .

All these observations suggest that there are significant differences in the electrochemical signatures of  $\text{M(TPPP)}$  and  $\text{M(TPP)}$  but that all the observed electron transfers remain centered on the porphyrin ring in both series, except when  $\text{M} = \text{Co(II)}$ . The electron-withdrawing effect of the phosphorylated substituents is revealed in all cases with a significant shift of all waves towards more positive values, in some cases exceeding 100 mV.

### Optical properties and photostability

Electronic absorption spectra of  $\text{M(TPPP)}$  were recorded in diluted  $\text{CH}_2\text{Cl}_2$  and MeCN solutions at room temperature in air. The data collected for these complexes are listed in Table 2, together with those of related non-phosphonated porphyrins  $\text{M(TPP)}$ .

**Table 2.** Selected photophysical parameters for  $\text{M(TPPP)}$  and  $\text{M(TPP)}$ .

Compound	Solvent	Absorption, $\lambda_{\text{abs}}$ (nm) ( $\epsilon \cdot 10^{-3}$ ( $\text{M}^{-1} \text{cm}^{-1}$ ))	Fluorescence <sup>a</sup>	
			$\lambda_{\text{f}}$ (nm)	$\Phi_{\text{f}}$ <sup>b</sup>
$\text{H}_2(\text{TPPP})$	$\text{CH}_2\text{Cl}_2$	417, 513, 550, 590, 645		
	MeCN	357 (15), 416 (340), 482 (3), 513 (15), 546 (6), 587 (4), 642 (3)	646, 713	0.09
	MeCN/ $\text{H}_2\text{O}$ (10:1 v/v)		649, 714	0.07
$\text{H}_2(\text{TPP})^{\text{c}}$	MeCN	417 (575) <sup>d</sup> , 513 (14), 549 (5), 592 (5), 646 (4)	654, 720	0.09 <sup>e</sup>
$\text{Pd(TPPP)}$	$\text{CH}_2\text{Cl}_2$	415 (275), 522 (25), 554 (3)		
	MeCN	413 (253), 523 (22), 552 (3)	665, 604	0
$\text{Pd(TPP)}^{\text{f}}$	toluene	417 (257), 485 (2), 523 (26), 554 (1)	560, 607	0
$\text{In(TPPP)}$	$\text{CH}_2\text{Cl}_2$	404 (40), 426 (6167), 518 (3), 559(21), 598 (8)	603, 657	
	MeCN	403 (36), 423 (1080), 518 (3), 559(21), 598 (8)	606, 661	0.01
$\text{In(TPP)}$	$\text{CH}_2\text{Cl}_2$	403 (35), 425 (1176), 520 (3), 560 (19), 599 (8)	604, 660	
	ethanol			0.01 <sup>g</sup>
$\text{Co(TPPP)}$	$\text{CH}_2\text{Cl}_2$	412 (251), 438 (28), 528 (16)	-	-
$\text{Co(TPP)}^{\text{h}}$	$\text{CH}_2\text{Cl}_2$	412, 528	-	-
$\text{Zn(TPPP)}$	$\text{CH}_2\text{Cl}_2$	423 (380), 550 (17), 592 (sh)		
	MeCN		604, 657	0.04
$\text{Zn(TPP)}^{\text{c}}$	MeCN	420 (661), <sup>i</sup> 556 (20), 596 (7)	604, 652	0.03 <sup>j</sup>

H <sub>2</sub> (TPPP-A)	MeCN/H <sub>2</sub> O <sup>k</sup> (1:1 v/v)	399 (67), 416 (346), 482 (3), 516 (13), 552 (8), 589 (4), 644 (4)	649, 714	0.11
Pd(TPPP-A)	MeCN/H <sub>2</sub> O <sup>k</sup> (1:1 v/v)	415 (213), 463 (6), 523 (17), 556 (2)	564, 607	0

<sup>a</sup> Emission was excited at 556 nm for all compounds studied in this work with the exception of Pd(II) complexes which were excited at 523 nm (Q(0,0)). <sup>b</sup> Fluorescence quantum yield were measured at ambient temperature relative to a solution of Zn(TPP) in MeCN as a standard. <sup>c</sup> Absorption and emission properties from ref. 65 <sup>d</sup> Average value of 418 (458) was found from all data previously reported<sup>66</sup> limited to consistent values. <sup>e</sup> Ref. 67. Average value 0.14 was calculated from all previously reported data<sup>66</sup> limited to consistent values. <sup>f</sup> Ref. 67, 68. <sup>g</sup> Ref. 69. Quantum yield for this compound in DMSO is 0.05.<sup>70</sup> <sup>h</sup> Ref. 71. <sup>i</sup> Average value of 421 (57) was found from all previously reported data<sup>66</sup> limited to consistent values. <sup>j</sup> Ref. 72. <sup>k</sup> A starting solution of M(TPPP-A) were prepared diluting the solution of porphyrin in 0.1 M NaOH (1mL) by MeCN (10 mL) and water (9mL). A MeCN/H<sub>2</sub>O solvent mixture (1:1 v/v) was used for further dilutions of this solution.

All studied P(O)(OEt)<sub>2</sub>-substituted porphyrins exhibit similar absorption shapes to the non-phosphonated M(TPP) analogues (Fig. S14<sup>†</sup>). This reveals the absence of significant alterations in the electronic transitions resulting from the *para*-substitution of the lateral phenyl substituent by phosphonate groups, in accordance with DFT calculations of M(TPPP) (M = H<sub>2</sub>, Pd, InCl) (Fig. 2). The expected number of intensive Q bands decrease predictably from four to two upon the insertion of metal ions into the macrocycle, reflecting a change in molecular symmetry from *D*<sub>2h</sub> to *D*<sub>4h</sub>.<sup>73,74</sup>

In the case of Co(TPPP), the position of the Soret band was close to those observed for other Co(II) complexes with 5,10,15,20-tetraarylporphyrins bearing electron-deficient substituents.<sup>75</sup> As expected, the absorption maximum of Pd(TPPP) appeared blue-shifted compared to those of Zn(TPPP).<sup>67</sup> This blue shift was accompanied by a decrease in the extinction coefficient coming along with an increase in the full-width-at-half-maximum of the Soret band, as previously observed for Pd(II) complexes with different porphyrin ligands.<sup>67</sup>

As reported in literature for related compounds,<sup>76</sup> all synthesized M(TPPP) displayed negligible solvatochromic properties (Table 2). In our case, it suggests the absence of axial coordination of phosphonate groups to the central metal ions and the non-dissociation of the axial chloride ion in In(TPPP). This conclusion is further supported by a good linearity observed between absorption and concentration for all studied compounds (Fig. S15<sup>†</sup>).

Spectroscopic properties of the water-soluble porphyrins H<sub>2</sub>(TPPP-A) and Pd(TPPP-A) were investigated in MeCN/H<sub>2</sub>O (1:1 v/v) solvent mixture (Table 1) and in pure water (Fig. S16–S19<sup>†</sup>). The compounds were soluble only under slightly basic conditions and a good linear correlation between absorption and concentration was observed for all bands in the concentration range of 5·10<sup>-7</sup>–10<sup>-4</sup> M (Fig. S17 and S19<sup>†</sup>). No evidence of aggregation was



thus observed when studying these porphyrins even in aqueous media, which constitutes an essential prerequisite for subsequent photophysical studies and catalytic experiments.

Emission properties of M(TPPP) and M(TPPP-A) were next investigated in MeCN and in MeCN/H<sub>2</sub>O solvent mixtures at 298 K (Table 2). Upon excitation in the Q bands, the free base porphyrin H<sub>2</sub>(TPPP) exhibited two fluorescence bands (Q(0,0) and Q(0,1)). The position of the maxima of these bands did not change after the addition of *ca.* 10 vol% of water to the studied solution. However, the fluorescence quantum yield ( $\Phi_f$ ) decreased from 0.09 to 0.07 after this addition due to the quenching effect of water molecules. Interestingly, the emission intensity of the phosphonate-substituted porphyrin H<sub>2</sub>(TPPP-A) in the MeCN/H<sub>2</sub>O mixture (1:1 v/v) was higher ( $\Phi_f = 0.11$ ) than that of H<sub>2</sub>(TPPP) in the MeCN/H<sub>2</sub>O mixture (10:1 v/v) ( $\Phi_f = 0.07$ ), despite the elevated water content in the solvent mixture. The emissivity of H<sub>2</sub>(TPPP-A) under these experimental conditions was comparable to that of either H<sub>2</sub>(TPPP) or H<sub>2</sub>(TPP) in MeCN.

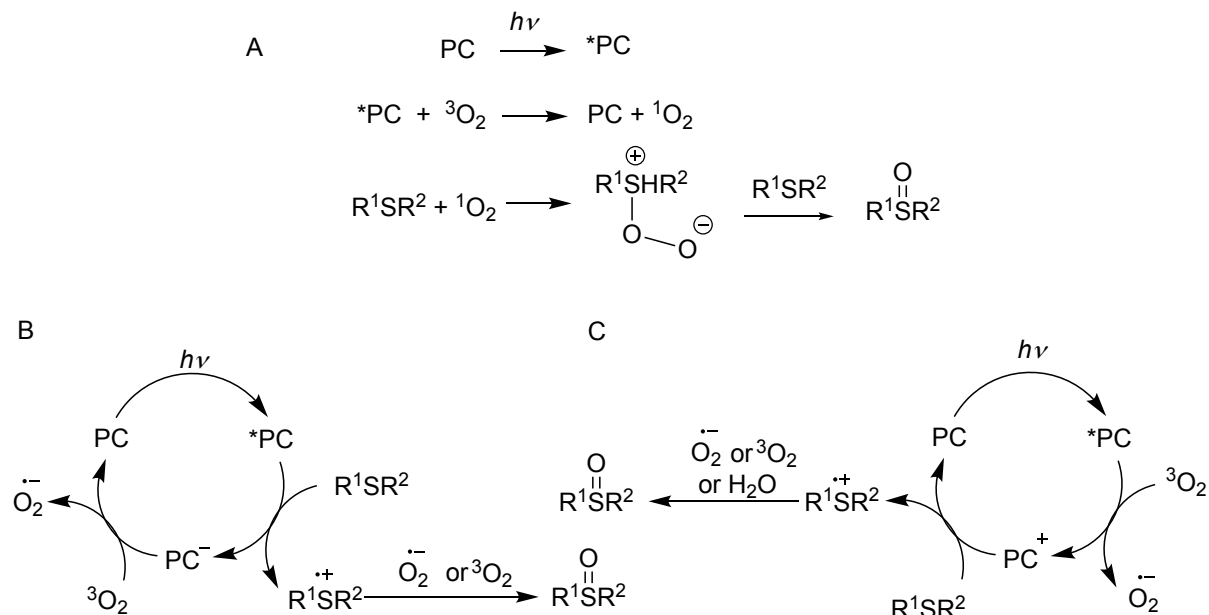
The emission properties of M(TPPP) complexes were highly dependent on the central metal ion while being similar to those of the reference TPP-based complexes. Co(TPPP) and Cu(TPPP) were non-emissive, as expected for open-shell paramagnetic metal complexes. The emission spectra of Zn(II), Pd(II), and In(III) porphyrins in aerated solution were dominated by S<sub>1</sub> → S<sub>0</sub> fluorescence, but the fluorescence quantum yields in the M(TPPP) series, as well as in the case of Pd(TPPP-A), were significantly reduced compared to those of the corresponding free base porphyrins. This decrease in  $\Phi_f$  was attributed to the presence of the metal ion, which promotes intersystem crossing due to strong spin-orbit coupling (so-called “the heavy atom effect”).<sup>73,77</sup> For our compounds, this was experimentally demonstrated by studying their emission in solutions that were deoxygenated under reduced pressure (10<sup>-2</sup> mm Hg). The normalized emission spectra of Pd(TPPP-A) in degassed MeCN/H<sub>2</sub>O (1:1 v/v) solution is shown in Fig. S20<sup>†</sup>. A moderate phosphorescence was observed at 785 nm (T<sub>1</sub>→S<sub>0</sub> transition), and its intensity decreased rapidly and almost fully quenched (with an efficiency above 99%), upon exposure of the solution to air. Similar behavior was observed for In(TPPP) but the intensity of the phosphorescence was weaker compared to Pd(TPPP), consistent with this complex having a heavier metal atom than In(TPPP), thereby favoring radiative processes for the T<sub>1</sub>→S<sub>0</sub> transition.

Thus, the introduction of diethyl phosphonate groups at the periphery of the tetrapyrrolic macrocycle and the subsequent hydrolysis of these groups to phosphonic acid did not cause significant changes in the photophysical properties of the tetrapyrrolic macrocycles, regardless

of the central metal ions present. These data reveal the potential interest of compounds prepared in this study for developing reusable photocatalysts.

### Catalytic reactions

Photocatalytic properties of porphyrins from the M(TPPP) series were investigated in the oxidation of sulfides to sulfoxides. This reaction has gained significant attention due to its relevance in various fields, including natural processes, organic synthesis, warfare agent disposal, and fuel desulfurization.<sup>78–82</sup> The oxidation of sulfides often leads to overoxidation to sulfones and the undesired cleavage of S–C and (S)C–H bonds. Thus, the development of selective methods for preparing sulfoxides under mild conditions is of great interest.<sup>83–86</sup> Photocatalytic reactions allow to perform this transformation using molecular oxygen as a terminal oxidant, thereby eliminating the need for strong and toxic oxidizing agents.<sup>87–89</sup> Substantial efforts have been dedicated to optimizing this reaction, which can proceed through energy transfer (EnT, to molecular oxygen (<sup>3</sup>O<sub>2</sub>) to generate singlet oxygen (<sup>1</sup>O<sub>2</sub>)) (Scheme 3A)) or electron transfer (ET, either to the substrate (Scheme 3B) and/or to molecular oxygen to form superoxide (Scheme 3C)) mechanisms, depending on the nature of the photocatalyst (PC) and the sulfide.<sup>90–93</sup>



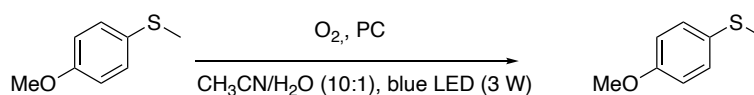
**Scheme 3.** Representation of mechanisms of photocatalytic oxidation of sulfides by molecular oxygen proceeding through energy transfer (A) and electron transfer (B and C).

In order to facilitate these reactions, photocatalysts (PC) that efficiently generate triplet excited states are highly essential. In many cases, heavy-metal complexes (Ir(III), Ru(II)) with

polypyridine ligands or halogen-substituted chromophores (Eosin, Rose Bengal, and so forth) are employed as PCs to promote intersystem crossing, benefiting from the heavy atom effect. However, these compounds come with inherent limitations such as toxicity, production costs, or specific excitation wavelengths. Although porphyrin derivatives, which serve as archetypical  $^1\text{O}_2$  photosensitizers in the context of photodynamic therapy (PDT), have also been utilized as PCs for this transformation, their practical application is still in the early stages of development.<sup>94</sup>

One of the primary challenges associated with use of porphyrins as PCs is their low solubility in many organic solvents. As a result, homogeneous reactions using porphyrin PCs are often performed in chlorinated solvents, employing specific derivatives prepared through complex multistep synthetic procedures.<sup>14,95–97</sup> To overcome these drawbacks, researchers have focused on developing efficient methods for their heterogenization<sup>98–105</sup> and have explored the replacement of porphyrins with alternative organic dyes or materials, even though these dyes generally possess less favorable light-absorbing properties and photostability.<sup>106–111</sup> Within this context, the availability and improved solubility of porphyrins prepared in this work make them promising candidates for performing various homogeneous photocatalytic processes, including the sulfoxidation reaction.

To explore their potential, we firstly compared these catalysts with palladium(II) *meso*-tetra(pentafluorophenyl)porphyrinate (Pd(F<sub>20</sub>TPP)), which was reported as an efficient PC for oxidation of sulfides.<sup>61</sup> A solution of 4-methoxythioanisole and Pd(F<sub>20</sub>TPP) (0.05 mol%) in MeCN (HPLC-grade) was stirred while slowly bubbling oxygen and irradiated with a blue LED (450 nm, 3 W). Surprisingly, under these conditions, no oxidation was observed, in contrast to what was reported previously<sup>61</sup> (Table 3, entry 1). However, when water was added as a co-solvent at a 10:1 ratio (v/v)<sup>112</sup> the starting sulfide was consumed after 8 h of irradiation (Table 3, entry 2). As shown in Table 3, Pd(TPPP) displayed higher efficiency, affording the desired sulfoxide quantitatively after only 1.5 h of irradiation (entry 3). Remarkably, when this complex was replaced by the less costly and more environmentally friendly free base porphyrin H<sub>2</sub>(TPPP), the rate and selectivity of the oxidation reaction did not decrease significantly (entry 4). The replacement of Pd(F<sub>20</sub>TPP) with the free base porphyrin H<sub>2</sub>(F<sub>20</sub>TPP) was not feasible because H<sub>2</sub>(F<sub>20</sub>TPP) is insoluble in MeCN, and the addition of water does not improve its solubility.

**Table 3.** Photooxidation of 4-methoxythioanisole in the presence of M(TPPP) and Pd(F<sub>20</sub>TPP).<sup>a</sup>

	Catalyst	Loading (mol%)	Time (h)	Conversion <sup>b</sup> (%)	Yield <sup>b</sup> (%)	
					Sulfoxide	Sulfone
1 <sup>c</sup>	PdF <sub>20</sub> TPP	0.05	3	1	1	0
2		0.05	2	21	21	0
			5	70	70	0
			8	100	99	1
3 <sup>d</sup>	Pd(TPPP)	0.05	1.5	100	100	0
4	H <sub>2</sub> (TPPP)	0.05	2	100	99	1
5	-		12	0	0	0
6	Co(TPPP)	0.15	12	1	1	0
7	Cu(TPPP)	0.15	12	0	0	0
8 <sup>d</sup>	Zn(TPPP)	0.05	4	2	20	1
9 <sup>d</sup>	In(TPPP)	0.05	2	47	47	0
			3.5	100	99	1

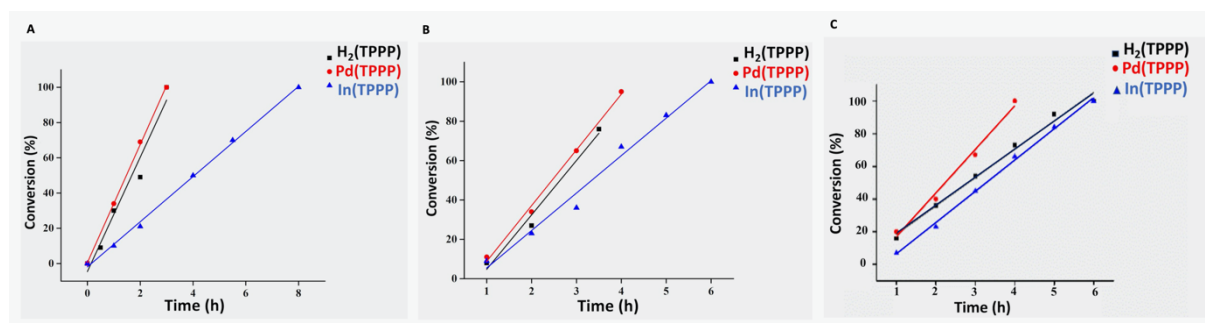
<sup>a</sup> Reaction conditions: 0.5 mmol of sulfide and PC were stirred and irradiated by blue LED (450 nm, 3 W) in MeCN/H<sub>2</sub>O mixture (2.75 mL, 10:1 v/v) bubbling slowly molecular oxygen at room temperature. <sup>b</sup> Conversion and selectivity were determined by <sup>1</sup>H NMR analysis of reaction mixtures using toluene as an internal standard. <sup>c</sup> The experiment was conducted in MeCN (2.75 mL). <sup>d</sup> The reaction didn't proceed without irradiation of the reaction mixture.

In a next series of experiments, we investigated the photocatalytic activity of Co(II), Cu(II), Zn(II) and In(III) complexes conducting the oxidation in MeCN/H<sub>2</sub>O mixture (Tables 3). The desired product was obtained in good yields only using metalloporphyrinates known for their ability to generate singlet oxygen, e. g. Zn(II) and In(II) complexes (entries 8 and 9). In independent experiments conducted with these complexes, we confirmed that no reaction takes place in the absence of appropriate irradiation and under irradiation of the reaction mixture without adding PC (entry 5).

To choose PC and solvent for recycling development, the photostability of H<sub>2</sub>(TPPP) and its Zn(II), Pd(II) and In(III) in CH<sub>2</sub>Cl<sub>2</sub>, MeCN and MeOH was investigated. In these experiments, solutions of M(TPPP) were stirred under irradiation with a blue LED (450 nm, 3 W) during several days monitoring their light absorption by UV-vis spectroscopy. As shown in Fig. S21<sup>†</sup>, all the compounds under investigation were rapidly decomposed in CH<sub>2</sub>Cl<sub>2</sub>. Accordingly, chlorinated solvents are inappropriate for photocatalytic reactions or recycling, as prolonged irradiation is generally required. Irradiation in MeOH and MeCN also causes a rapid

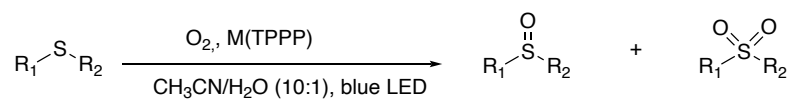
decomposition of Zn(TPPP), but other porphyrins were found to be remarkably stable, as revealed by minor decreases (less than 10%) in their light absorbance after 2 d of irradiation.

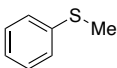
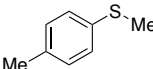
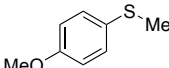
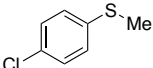
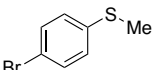
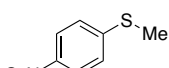
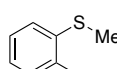
Zn(TPPP) was thus excluded from subsequent studies focusing on selectivity and the oxidation kinetics of dibutyl sulfide and two differently functionalized aryl methyl sulfides, namely 4-methoxythioanisole and 4-chlorothioanisole, using H<sub>2</sub>(TPPP) or its In (III) and Pd(II) complexes (Fig. 7). These specific substrates were chosen because they are known to react with molecular oxygen through different mechanisms.<sup>91,92</sup> While singlet oxygen generation is reported as the main pathway involved in the sulfoxidation of dialkyl sulfides (Scheme 3, pathway A), other aryl methyl sulfides tend to react through both energy transfer (EnT) and electron transfer (ET) processes (Scheme 3, pathways B and C). Consequently, the PC efficiency may differ for these three substrates. All our experiments show that In(TPPP) is less efficient than Pd(TPPP) and H<sub>2</sub>(TPPP), both of which exhibit similar catalytic activities (Fig. 7).

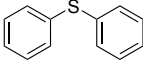
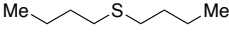
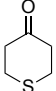
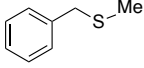


**Fig. 7** Comparative studies of catalytic efficiency of M(TPPP) in the oxidation of 4-methoxythioanisole (A), 4-chlorothioanisole (B) and dibutyl sulfide (C) by molecular oxygen in a MeCN/H<sub>2</sub>O solvent mixture (10:1 v/v) under irradiation with a blue LED (450 nm, 3 W).

H<sub>2</sub>(TPPP) and Pd(TPPP) were thus selected for investigating substrate scope using 0.05 mol% of porphyrin PCs. The results obtained in this study are summarized in Table 4. When H<sub>2</sub>(TPPP) was used as photocatalyst, all aryl methyl sulfides were transformed to sulfoxides selectively and almost quantitatively although the reaction time was varied (entries 1, 3, 4, 8 and 11). Electron-rich sulfides exhibited higher reactivity than those containing electron-deficient aryl groups. Such a trend in the evolution of reactivity is expected whether the reactions proceed through generation of electrophilic singlet oxygen in EnT process (Scheme 3, pathway A)<sup>113</sup> or through ET (Scheme 3, pathways B and C).<sup>112</sup> Notably, the catalyst loading could be halved with a corresponding increase in reaction time (entries 4 and 5, 8 and 9). Bulky *ortho*-bromothioanisole was also selectively photooxidized to sulfoxide, although after 7 h of irradiation (entry 16). The nitro-substituted derivatives, known for their inertness in EnT reactions,<sup>112</sup> exhibited significantly slower reaction rates, as revealed by the 45% conversion

**Table 4.** Photooxidation of sulfides in the presence of H<sub>2</sub>(TPPP) and Pd(TPPP).<sup>a</sup>

Entry	Sulfide	Catalyst M(TPPP) (mol%)	Time (h)	Conversion <sup>b</sup> (%)	Yield <sup>b</sup> (%)	
					Sulfoxide	Sulfone
1		H <sub>2</sub> (TPPP) (0.05)	2.5	100	98	2
2		Pd(TPPP) (0.05)	3	100	98	2
3		H <sub>2</sub> (TPPP) (0.05)	2.5	100	99	1
4		H <sub>2</sub> (TPPP) (0.05)	2	100	99	1
5		(0.025)	3	100	97	3
6		Pd(TPPP) (0.05)	1.5	100	100	0
7		(0.025)	2.5	100	100	0
8		H <sub>2</sub> (TPPP) (0.05)	2.5	100	100	0
9		(0.025)	4.5	100	99	1
10		Pd(TPPP) (0.025)	4.5	100	100	0
11		H <sub>2</sub> (TPPP) (0.025)	4.5	100	99	1
12		Pd(TPPP) (0.025)	4.5	100	100	
13		H <sub>2</sub> (TPPP) (0.05)	8	45	100	0
14 <sup>3</sup>		(0.05)	1.5	100	100	0
15 <sup>3</sup>		Pd(TPPP) (0.05)	1.5	100	100	0
16		H <sub>2</sub> (TPPP) (0.05)	7	100	98	2
17		Pd(TPPP)	7	100	99	1

		(0.05)				
18		H <sub>2</sub> (TPPP)				
		(0.05)	5	0	0	0
19 <sup>c</sup>		(0.05)	5.5	99	97	2
20 <sup>c</sup>		Pd(TPPP)				
		(0.05)	5.5	99	97	2
21		H <sub>2</sub> (TPPP)				
		(0.005)	4	100	99	1
22		Pd(TPPP)				
		(0.005)	4	100	100	0
23		H <sub>2</sub> (TPPP)				
		(0.005)	4	40	40	0
24		(0.01)	4	100	98	2
25		H <sub>2</sub> (TPPP)				
		(0.005)	7	100	99	1

<sup>a</sup> Reaction conditions: 0.5 mmol of sulfide and PC were stirred and irradiated by blue LED (450 nm, 3 W) in MeCN/H<sub>2</sub>O mixture (2.75 mL, 10:1, v/v) bubbling slowly molecular oxygen at room temperature. <sup>b</sup> Conversion and selectivity were determined by <sup>1</sup>H NMR analysis of reaction mixtures using biphenyl as an internal standard. <sup>c</sup> The reaction was conducted in EvoluChem Photoredox box using blue LED (450 nm, 30 W).

obtained after 8 h of irradiation (entry 13). However, the kinetics could be improved by conducting the reaction in a closed vessel under oxygen (balloon of 1L) under irradiation in a commercially available EvoluChem Photoredox box (entry 14). The later combines a powerful blue LED (450 nm, 30 W) and a mirror system for optimizing light distribution. Remarkably, even diphenyl sulfide, which is known for its high photostability due to its low nucleophilicity and steric hindrance, could be efficiently oxidized using H<sub>2</sub>(TPPP) under these irradiation conditions, yielding diphenylsulfoxide in 97% after only 5.5 h of irradiation (entries 18 and 19). Dibutyl sulfide was oxidized more rapidly compared to all aryl methyl sulfides. When the amount of catalyst was reduced by a factor of 10 (0.005 mol%), the oxidation reaction was completed within 4 h (entry 21). The cyclic thian-4-one exhibited lower reactivity than dibutyl sulfide (entry 23) but it was nevertheless successfully oxidized in 4 h in the presence of 0.01 mol% of the photocatalyst (entry 24). Another important result for the synthetic applications is that the selectivity of sulfoxidation remains unchanged even for benzyl methyl sulfide – a compound known to produce many by-products during photocatalytic oxygenation (entry 25).

Similar results were obtained when employing the free base porphyrin H<sub>2</sub>(TPPP) instead of its Pd(II) complex. (Table 4, entries 2, 6, 7, 10, 12, 15, 17, 19 and 22). The costs associated with the insertion of palladium into the macrocycle were balanced by a slight acceleration of the reaction rate and a minor increase in selectivity of the oxidation.

Comparing the reactivity of different types of sulfides and efficiency of Pd(TPPP) and H<sub>2</sub>(TPPP), we hypothesized that the sulfoxidation reaction in the presence of M(TPPP)

primarily proceeds through the EnT mechanism (Scheme 3, pathway A). To better understand the reaction pathway, we investigated the efficiency of singlet oxygen generation by M(TPPP) *via* photophysical and EPR measurements.

The photophysical measurements were carried out in CD<sub>3</sub>CN/D<sub>2</sub>O (10:1 v/v) by direct detection of the singlet oxygen phosphorescence signal at 1270 nm. Since the singlet oxygen quantum yield ( $\varphi_{\Delta}$ ) of **PH** has never been reported in MeCN/H<sub>2</sub>O mixtures to our knowledge, we assigned this value to be equal to that reported in the literature for many other non-polar or polar solvents ( $\varphi_{\Delta} = 0.95$ ).<sup>114</sup> With this value in hand, we showed that both In(TPPP) and Pd(TPPP) exhibited, within error margin, a quasi-unitary singlet oxygen sensitization quantum efficiency (measured  $\varphi_{\Delta} = 0.94$  and 1.01, respectively). The singlet oxygen quantum yield of the free base porphyrin H<sub>2</sub>(TPPP) ( $\varphi_{\Delta} = 0.72$ ), although still significantly higher than that reported for most free base porphyrins ( $\varphi_{\Delta} = 0.50$ – $0.60$ <sup>115</sup> for H<sub>2</sub>(TPP), being the most studied analogue), was lowered than those of Pd(II) and In(III) complexes pointing out the heavy-atom effect on the intersystem crossing efficiency (Table 5 and Fig. S22<sup>†</sup>).

The potential involvement of ET on the substrates was also investigated by tracing the evolution of the emission intensity upon the gradual addition of 4-methoxythioanisole into degassed solution of Pd(TPPP). Quenching of the phosphorescence band was observed, together with a shortening in phosphorescence lifetime, albeit only at very high substrate concentrations. A Stern-Volmer plot built from those experimental data allowed to calculate a quenching constant  $k_q$  of  $3 \cdot 10^7 \text{ M}^{-1} \text{ s}^{-1}$ , almost three orders of magnitude below that generally considered for diffusion-controlled processes. These results are thus revealing that ET on substrate (Scheme 3, pathway B) is highly unlikely to occur in the oxidation of 4-methoxythioanisole, and that the oxidation is likely dominated by the singlet oxygen pathway, even for aryl sulfides.

The experimental conditions implemented for photophysical measurements, as discussed above, differ significantly from the conditions used for catalytic tests. An alternative approach to study oxidation reactions involves use of EPR spectroscopy measurements, which allows to obtain key information on the generation of singlet oxygen in non-deuterated solvents and under *operando* conditions, by irradiating the samples in the cavity of the EPR spectrometer.<sup>116–118</sup>

In this work, we explored the potential of EPR/spin trapping techniques for the quantification of singlet oxygen generation, with the aim of establishing a relatively inexpensive and practical procedure, requiring small quantities of PC (measurements done in capillary tubes,  $V < 0.1 \text{ mL}$ ). The commonly used 2,2,6,6-tetramethylpiperidine (TEMP) spin



trap was selected, and the first series of measurements was conducted in MeCN under irradiation with 365 nm LED positioned near the EPR cavity (refer to the Experimental Section for details). The rate of TEMPO formation in the presence of **PH**, H<sub>2</sub>(TPPP), Pd(TPPP), and In(TPPP) was measured, and  $\phi_{\Delta}$  values were calculated, considering phenalene-1-one ( $\phi_{\Delta} = 1.00^{114}$ ) as a standard compound (see ESI). The main results of these studies are shown in Table 5. The data obtained through the EPR/spin trapping method align well with those acquired through singlet oxygen phosphorescence measurements. However, when the same series of experiments was conducted in a MeCN/H<sub>2</sub>O solvent mixture (10:1 v/v), the  $\phi_{\Delta}$  of **PH** was significantly lower than those of Pd(TPPP) (Fig. S24<sup>†</sup>). Further studies aimed at evaluating the photostability of **PH** in both solvents, in the absence and presence of TEMP (Fig. S25<sup>†</sup>), revealed that the photodecomposition of PH in acetonitrile is only slightly accelerated in the presence of water and that this rate is significantly increased after the addition of TEMP. This decomposition, found to be fast in aqueous MeCN, appears to be responsible for the decrease in singlet oxygen quantum yield in the presence of **PH**. These studies thus demonstrate that, **PH**, which is widely used as a standard compound in photophysical studies, can only serve as a standard for a rough estimation of the order of magnitude of  $\phi_{\Delta}$  calculated from EPR/spin trapping measurements. The EPR-spectroscopy procedure should be optimized in the future to provide quantitative data.

**Table 5.** Singlet oxygen quantum yields of M(TPPP) and **PH**.<sup>a</sup>

Compound	Solvent	$\phi_{\Delta}$ ( <sup>1</sup> O <sub>2</sub> emission)	$\phi_{\Delta}$ (EPR)
<b>PH</b>	CD <sub>3</sub> CN/D <sub>2</sub> O	0.95	
	MeCN		1.00 <sup>b</sup>
H <sub>2</sub> (TPPP)	CD <sub>3</sub> CN/D <sub>2</sub> O	0.72	
	MeCN		0.79
Pd(TPPP)	CD <sub>3</sub> CN/D <sub>2</sub> O	0.94	
	MeCN		0.92
In(TPPP)	CD <sub>3</sub> CN/D <sub>2</sub> O	1.01	
	MeCN		0.97

<sup>a</sup> Comparative study by singlet oxygen phosphorescence measurements and the EPR/spin trapping technique using TEMP as a spin trap (see, ESI for further details). <sup>b</sup> Ref. 114.

Altogether, our studies demonstrated that M(TPPP) are efficient singlet oxygen photosensitizers and that the EnT mechanisms seems to be predominant in our experimental conditions. Remarkably, despite singlet oxygen quantum yield of H<sub>2</sub>(TPPP) was much lower

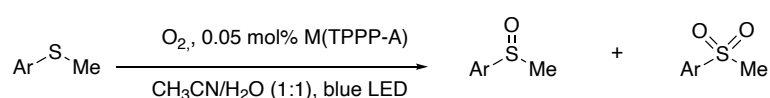
than that of Pd(TPPP), the catalytic efficiency of these two photosensitizers are rather similar likely due higher light absorption of H<sub>2</sub>(TPPP) in the working region of blue LED (Table 2).

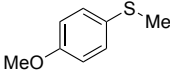
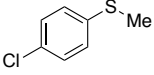
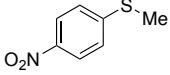
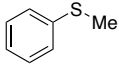
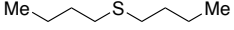
Finally, we looked at strategies for recovering and reusing the porphyrin PCs. Porphyrins bearing phosphonic acid functional groups, such as H<sub>2</sub>(TPPP-A) and Pd(TPPP-A), are soluble in water over a wide pH range allowing deprotonation of the phosphonic acid groups (pH > 2). In contrast, the targeted sulfoxides are commonly insoluble in water and can be extracted after reaction completion into polar organic phases such as chlorinated solvents or ethers. The aqueous phase containing the PC can then be utilized in a consecutive catalytic cycle. With this in mind, we investigated the photocatalytic properties of H<sub>2</sub>(TPPP-A) and Pd(TPPP-A) to propose a practical recycling procedure for the oxidation of sulfides.

To facilitate catalyst recycling, the reaction conditions were modified by increasing amount of water in the reaction mixture. The oxidation of 4-methoxythioanisole in the presence of M(TPPP-A) (0.05 mol%) was performed in a MeOH/H<sub>2</sub>O (1:1 v/v) solvent mixture keeping other experimental conditions unchanged (Table 6, entry 1 and 2). These conditions were chosen to allow a recycling of the aqueous phase containing the PC without going through evaporation. Under these conditions, the oxidation proceeded rapidly, but selective formation of the sulfoxide was observed only with Pd(TPPP-A). Use of H<sub>2</sub>(TPPP-A) led to an overoxidation of the sulfone. This side-reaction was observed even at relatively low conversion of the starting compound, indicating that controlling the reaction time alone could not increase the selectivity of this transformation. Similar results were obtained when studying the oxidation of 4-chlorophenyl methyl sulfide, although the reaction rate was decreased (entries 3 and 4). Intense irradiation (30 W) of the less reactive 4-nitrophenyl sulfide in the presence of H<sub>2</sub>(TPPP-A) gave only the sulfoxide, but the oxidation reaction was very slow (entries 5 and 6). The efficiency of Pd(TPPP-A) as a photosensitizer was also tested in the sulfoxidation of thioanisole (entry 7) and dialkyl sulfides, specifically by studying the oxidation of dibutyl sulfide (entry 8). Both reactions were successful and proceeded without any complications.

Once again, the mechanism underlying the photocatalytic properties of water-soluble porphyrins was investigated through photophysical measurements. Experimental conditions remained consistent with those described above, except for using a 1:1 CD<sub>3</sub>CN/D<sub>2</sub>O mixture as a solubilizing medium. Comparing to **PH** as a reference, slightly lower  $\phi_{\Delta}$  values were obtained

**Table 6.** Photooxidation of sulfides in the presence of H<sub>2</sub>(TPPP-A) and Pd(TPPP-A).<sup>a</sup>



Entry	Sulfide	Catalyst (mol%)	Time (h)	Conversion <sup>b</sup> (%)	Yield <sup>b</sup> (%)	
					Sulfoxide	Sulfone
1		H <sub>2</sub> (TPPP-A)	2	62	52	11
			3	100	68	32
2		Pd(TPPP-A)	3	100	100	0
3		H <sub>2</sub> (TPPP-A)	16	65	41	24
4			Pd(TPPP-A)	7	100	100
5 <sup>c</sup>		H <sub>2</sub> (TPPP-A)	1	6	6	0
			4	24	24	0
			20	86	86	0
			28	89	89	0
6		Pd(TPPP-A)	1	100	100	0
7		Pd(TPPP-A) <sup>d</sup>	4	100	100	0
8		Pd(TPPP-A) <sup>d</sup>	1	100	100	0

<sup>a</sup> Reaction conditions: 0.5 mmol of sulfide and pPC were stirred and irradiated by blue LED (450 nm, 3 W) in MeCN/H<sub>2</sub>O mixture (3 mL, 1:1 v/v) bubbling slowly molecular oxygen at room temperature. <sup>b</sup> Conversion and selectivity were determined by <sup>1</sup>H NMR analysis of reaction mixtures using biphenyl as an internal standard. <sup>c</sup> The reaction was conducted in EvoluChem Photoredox box using blue LED (450 nm, 30 W). <sup>d</sup> The recycled catalyst was used in this reaction.

for the phosphonic acids compared to their diester analogues. Specifically, the yield of Pd(TPPP-A) was reduced to 0.83, while that of H<sub>2</sub>(TPPP-A) reached only 0.5 (Fig. S23<sup>†</sup>). Despite this slight decrease, the EnT mechanism involving participation of <sup>1</sup>O<sub>2</sub> appears to be also predominant in the reaction with these PCs.

The reusability of Pd(TPPP-A) was explored in the series of consecutive experiments shown in Fig. 8.

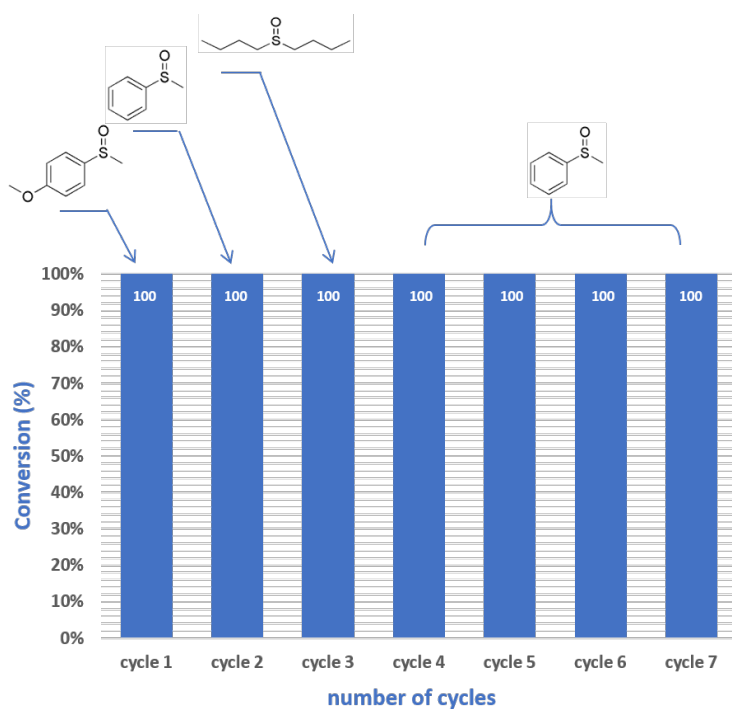


**Fig. 8.** Recycling Pd(TPPP-A) in the sulfoxidation reaction (Reaction conditions: 0.5 mmol of sulfide, 0.05 mol% of PC were stirred and irradiated by blue LED (450 nm, 3 W) in MeCN/H<sub>2</sub>O mixture (3 mL, 1:1, v/v) bubbling slowly molecular oxygen at room temperature).

In the first reaction, 4-methoxyanisol yielded the target sulfoxide in quantitative yield after 4 h of irradiation. The recovery of photocatalyst was straightforward. After the reaction was completed, the product was extracted with CH<sub>2</sub>Cl<sub>2</sub> and the remaining aqueous phase, containing the porphyrin catalyst, was reused in the next cycle. In this step, thioanisol was oxidized after 4 h of irradiation and the pure product was obtained in quantitative yield by extraction with CH<sub>2</sub>Cl<sub>2</sub>. The aqueous phase containing the photocatalyst was introduced in the next catalytic cycle to convert dibutyl sulfide into corresponding sulfoxide in quantitative yield after 1.5 h of irradiation. In the following three consecutive cycles, thioanisole was oxidized increasing the reaction time to 12 h to achieve a complete conversion without monitoring of the reaction mixture. The desired product was obtained quantitatively and isolated in pure form after extraction with CH<sub>2</sub>Cl<sub>2</sub>, without the need for additional chromatographic purification.

It is noteworthy that the photocatalytic properties of water-soluble Mn(III) complexes for oxygenation of unsaturated compounds was thoroughly investigated.<sup>119–121</sup> In the case of sulfonate-substituted porphyrin derivatives, it was shown that free-base porphyrins also can be used as PCs. These catalysts can be easily separated from the target products but their reuse was impossible probably due to their low photostability.<sup>119–121</sup> To our knowledge, we report

here the first example of an oxidation reaction in which water-soluble porphyrins can be recycled and reused.

## CONCLUSIONS

We have showed that phosphonate-substituted porphyrins are promising compounds for catalytic applications, addressing key challenges associated with porphyrin catalysts, such as their availability, photostability and solubility.

In these study, metal complexes of phosphonate-substituted porphyrin  $H_2(TPPP)$  were prepared in good yields by inserting Pd(II), In(III), and Co(II) ions in the free base porphyrin ligand. The photophysical properties, photostability, and redox behavior of the newly synthesized  $M(TPPP)$  complexes were thoroughly investigated. The introduction of the diethyl phosphonate group at the phenyl substituent significantly altered the electronic properties of the tetrapyrrolic macrocycle. The presence of these electron-withdrawing groups resulted in easier reductions and harder oxidations of the macrocycle for all complexes, compared to the corresponding TPP derivatives. Pd(TPPP) and In(TPPP) complexes in acetonitrile exhibited remarkably high single oxygen quantum yields and excellent photostability, while being soluble in non-chlorinated solvents such as acetonitrile and methanol.

The studies on the  $M(TPPP)$  porphyrins as PCs for the oxidation of sulfide have revealed that the free base porphyrin  $H_2(TPPP)$  and Pd(TPPP) are highly effective PCs for the sulfoxidation reaction, and that both operate with a mechanism dominated by a singlet oxygen oxidation pathway. Remarkably, photostability and catalytic efficiency of the free base porphyrin  $H_2(TPPP)$  are comparable to those of the more expensive Pd(TPPP) complex. Readily obtainable porphyrin  $H_2(TPPP)$  is among the best metal-free photocatalyst known for selective oxidation of sulfides to sulfoxides using molecular oxygen as a terminal oxidant.

To enhance the reaction sustainability, we explored the recovery of the porphyrin PC through a post-synthesis liquid phase-separation process. For this purpose, the best photocatalysts,  $H_2(TPPP)$  and Pd(TPPP), were converted into their water-soluble derivatives  $H_2(TPPP-A)$  and Pd(TPPP-A). These porphyrins were then investigated in the oxidation of sulfides. The oxidation reaction proceeded in MeCN/ $H_2O$  (1:1 v/v) in the presence both compounds, but selective transformation to the target sulfoxide was observed only with Pd(TPPP-A). The experimental procedure enables the straightforward recovery of the catalyst by extracting the product in  $CH_2Cl_2$ . The desirable sulfoxide can be isolated in its pure form by evaporating the organic phase thus obtained, without additional chromatographic purification. The aqueous phase, containing the PC, can be recycled and directly utilized in the subsequent

catalytic cycle. This strategy for the recovery of porphyrin photocatalysts offers an alternative approach to the extensively studied heterogenization of porphyrin PCs. Our research contributes to optimization of porphyrin photocatalysts, which exhibit excellent light absorbing properties and photostability.

## EXPERIMENTAL SECTION

### Synthesis

General information on materials, methods and synthesis of ligands and complexes M(TPPP) is present in the Supporting Information (ESI).

### DFT computations

To simplify the calculations ethyl substituents of phosphonate groups were replaced by methyl groups. The structure of M(TPPP-Me) was modeled by DFT calculations using the Firefly quantum chemistry package,<sup>122</sup> which is partially based on the GAMESS (US)<sup>123</sup> source code. The calculations were performed using the B3LYP functional with the Jorge-DZP basis set for all elements, at each step full optimization of geometry was achieved, and the minima were confirmed by computation of vibration frequencies.

### X-ray crystallography of Pd(TPPP-A)

Single clear dark violet needle-shaped crystals of (Me<sub>2</sub>NH<sub>2</sub>)<sub>2</sub>[Pd(TPPP-A)<sub>-2H</sub>] were recrystallised from a mixture of water and DMF (1:10 v/v) by slow evaporation. A suitable crystal with dimensions 0.43 x 0.18 x 0.13 mm<sup>3</sup> was selected and mounted on a MITIGEN holder oil on a Nonius Kappa Apex II diffractometer. The crystal was kept at a steady  $T = 110.0(1)$  K during data collection. The structure was solved with the ShelXT<sup>124,125</sup> solution program using dual methods and by using Olex2<sup>126</sup> as the graphical interface. The model was refined with ShelXL<sup>124,125</sup> using full matrix least squares minimisation on  $F^2$ .

*Crystal Data.* C<sub>48</sub>H<sub>45</sub>N<sub>6</sub>O<sub>12</sub>P<sub>4</sub>Pd,  $M_r = 1128.18$ , triclinic,  $P-1$  (No. 2),  $a = 13.0368(4)$  Å,  $b = 13.9158(5)$  Å,  $c = 18.0430(6)$  Å,  $\alpha = 69.419(2)^\circ$ ,  $\beta = 81.680(2)^\circ$ ,  $\gamma = 78.062(2)^\circ$ ,  $V = 2988.85(18)$  Å<sup>3</sup>,  $T = 110.0(1)$  K,  $Z = 2$ ,  $Z' = 1$ ,  $\mu(\text{Mo K}\alpha) = 0.474$ , 175832 reflections measured, 10535 unique ( $R_{\text{int}} = 0.0878$ ) which were used in all calculations. The final  $wR_2$  was 0.1521 (all data) and  $R_I$  was 0.0606 ( $I \geq 2 \sigma(I)$ ). Additional structural data are given in Fig. S1–S3<sup>†</sup> and Tables S1–S6<sup>†</sup>.

Data CCDC-2290735 also contain the supplementary crystallographic information for this paper. These data can be obtained free of charge from The Cambridge Crystallographic Data Centre via [www.ccdc.cam.ac.uk/data\\_request/cif](http://www.ccdc.cam.ac.uk/data_request/cif).

### Electrochemical and spectroelectrochemical characterization

Acetonitrile (Acros Organics, extra-dry with molecular sieves, water < 0.005%) was degassed using a freeze-pump-thaw procedure and used as is in a glove box under N<sub>2</sub>. Tetra-*n*-butylammonium hexafluorophosphate (TBAP) was prepared, purified and dried using standard procedures.

Cyclic voltammetry and voltammetry with rotating disc electrodes (RDE) were recorded using a SP300 Biologic potentiostat. Analytical studies were conducted under N<sub>2</sub> (glove box) in a standard three-electrodes electrochemical cell. Tetra-*n*-butylammonium hexafluorophosphate was used as supporting electrolytes (0.1 M). An automatic ohmic drop compensation procedure (biologic ZIR) was systematically performed when using cyclic voltammetry. Vitreous carbon ( $\varnothing = 3$  mm) working electrodes (CH Instruments) were polished with 1 mm diamond paste before each recording. Voltamperometry with a rotating disk electrode (RDE) was carried out with a radiometer (CTV101 radiometer analytical) equipment at a rotation rate of 500 rad min<sup>-1</sup> using a glassy carbon RDE tip ( $\varnothing = 3$  mm).

Spectroelectrochemical measurements were carried out at room temperature under N<sub>2</sub> (glove box) in dedicated batch “thin layer” type of cells (0.5 or 1 mm optical path lengths, Pt mesh electrodes, ALS Co. Ltd.) using a biologic SP300 potentiostat coupled to a MCS 601 UV-NIR Zeiss spectrophotometer. The counter-electrode was a platinum wire isolated from the electrolytic solution through an ionic bridge. Ag/AgNO<sub>3</sub> (CH Instruments, 10<sup>-2</sup> M + TBAP 10<sup>-1</sup> M in MeCN) was used as a reference electrode. Ferrocene was ultimately used as an internal reference. Measurements were carried out upon scanning the working electrode potential at 20 mV s<sup>-1</sup> between the open circuit potential and a chosen final potential followed by microelectrolysis (1–5 min) at this potential.

### **Photophysical measurements**

UV-vis spectra were recorded in solutions using a PerkinElmer Lambda 900 UV/VIS/NIR spectrometer (1 cm path length quartz cell). Emission spectra were measured using a Horiba Jobin Yvon Fluorolog-3 spectrometer. Emission quantum yields of all compounds were measured relative to the Zn(TPP) in acetonitrile ( $\Phi_f = 0.033$ )<sup>127</sup> and calculated using a standard procedure.<sup>128</sup>

Singlet oxygen emission spectra were measured using a Horiba Jobin Yvon Fluorolog-3 fluorimeter, equipped with a three-slit double-grating excitation and emission monochromator with a dispersion of 2.1 nm mm<sup>-1</sup> (1200 grooves mm<sup>-1</sup>). The steady-state luminescence was excited by unpolarized light from a 450 W xenon continuous wave (CW) lamp at the desired excitation wavelength, and with excitation slits opening of 10 nm. It was detected at an angle of 90° for measurements of dilute solutions (10 mm quartz cuvette, 15

nm emission slits opening, integration time = 1s) using a liquid nitrogen cooled solid indium/gallium/arsenide (InGaAs) detector (850–1600 nm). Spectra were corrected for both excitation source light-intensity variation and emission spectral responses (signal " $T_{1c}/R_{1c}$ ").

Singlet oxygen quantum yield ( $\varphi_{\Delta}$ ) measurements for M(TPPP) were achieved using a relative methodology based on the comparison of  $^1O_2$  phosphorescence intensity of diluted  $CD_3CN/D_2O$  (10:1 v/v) solutions (optical density (OD) < 0.1) of studied samples against that of phenalen-1-one (**PH**) in the same solvent ( $\varphi_{\Delta} = 0.95$ ) used here as a reference compound. Singlet oxygen luminescence quantum yields were calculated using the following equation

$$\varphi_{\Delta}^x = \varphi_{\Delta}^r \left[ \frac{A_r(\lambda_r)}{A_x(\lambda_x)} \right] \left[ \frac{I_x}{I_r} \right]$$

where  $A(\lambda)$  is the absorbance (or optical density) at the excitation wavelength and  $I$  the corrected integrated luminescence intensity. The subscripts r and x stand for reference and sample, respectively. The reported results are the average of 3–4 independent measurements at various absorbances (comprised between 0.01 and 0.1) for both sample and reference. The plot of the integrated luminescence intensity vs absorbance give straight line with excellent correlation coefficients and the associated slopes can be determined for both sample and reference, allowing straightforward determination of the sample  $^1O_2$  generation efficiency (Fig. S24†).

Singlet oxygen quantum yield ( $\varphi_{\Delta}$ ) measurements for M(TPPP-A) were carried out using the same methodology in  $CD_3CN/D_2O$  (1:1 v/v) solutions. pH was set basic by addition a droplet of NaOD in  $D_2O$ , in order to ensure full deprotonation of the phosphonate groups and avoid any aggregation of the porphyrin molecules, which could be highly detrimental for the reliability of the measurements. The results are summarized in Fig. S25†.

#### **Photocatalytic oxidation of sulfides**

Standard 0.01 M solutions of M(TPPP) in MeCN were prepared dissolving 0.05 mmol porphyrins in 5 mL volumetric flasks. Zn(TPPP) was employed as a powder due to its low solubility in MeCN, which significantly increased when dissolved in a MeCN/ $H_2O$  solvent mixture. Aqueous solution of M(TPPP-A) (0.01 M) was prepared dissolving the porphyrins M(TPPP-A) in 500  $\mu$ L of 0.1 N aqueous NaOH and diluted this solution by deionized water in 5 mL volumetric flasks.

*General procedure of sulfoxidation in the presence of M(TPPP).* A glass vial equipped with a magnetic stir bar was charged with 1 mmol of sulfide (see Tables 3 and 4) and calculated amount of standard solution of the photocatalyst. Then acetonitrile and water were added to



obtain the reaction mixture in acetonitrile/water mixture (2.75 mL, 10:1 v/v). The reaction was irradiated with blue LED while gently bubbling oxygen. When the reaction was complete, the mixture was diluted with 7 mL of water and extracted with dichloromethane ( $3 \times 5$  mL). The combined extracts were dried over sodium sulfate and evaporated under reduced pressure at room temperature. The yield and purity of the products were determined by  $^1\text{H}$  NMR using biphenyl as an internal standard.

Dibutyl sulfide was oxidized using 0.005 mol% of PCs, the oxidation of aryl sulfides was performed in the presence of 0.05 mol% of PCs. The catalyst loading and the reaction time are indicated in Tables 3 and 4.

This catalysts loading was also used in kinetic studies (Fig. 7) which were performed by using the same procedure. The reactions were periodically monitored by NMR spectroscopy after withdrawing aliquot samples.

*General procedure of sulfoxidation in the presence of M(TPPP-A).* A glass vial equipped with a magnetic stir bar was charged with 1 mmol of sulfide (see Table 6) and calculated amount of standard solution of the photocatalyst. Then MeCN and water were added to obtain the reaction mixture in MeCN/H<sub>2</sub>O mixture (2.75 mL, 1:1 v/v). The reaction was irradiated with blue LED while gently bubbling oxygen. When the reaction was complete, the mixture was diluted with 7 mL of water and extracted with dichloromethane (CH<sub>2</sub>Cl<sub>2</sub>,  $3 \times 5$  mL). The combined extracts were dried over sodium sulfate and evaporated under reduced pressure at room temperature. The yield and purity of the products were determined by  $^1\text{H}$  NMR using biphenyl as an internal standard.

The experiments with the recycled PC were performed using the same procedure. After reaction completion, the product was extracted with CH<sub>2</sub>Cl<sub>2</sub> ( $3 \times 5$  mL) and the aqueous phase containing PC was introduced in the next catalytic cycle.

### **Estimation of singlet oxygen generation using the EPR/spin trapping technique**

TEMP (Merck) was used as received. Quantitative studies were conducted to assess the generation of singlet oxygen by H<sub>2</sub>(TPPP), Pd(TPPP), and In(TPPP), utilizing TEMP as a spin trap in both MeCN and MeCN/H<sub>2</sub>O (10:1 v/v) solutions, in comparison to **PH**, which was dissolved in the same solvents. Two sets of four solutions, each with an equal absorption value ( $A = 0.45$ ) at 365 nm, were meticulously prepared by dissolving H<sub>2</sub>(TPPP), Pd(TPPP), In(TPPP), and **PH** in suitable solvents. Following this, 25 mM solutions of TEMP in the same solvents were prepared, and an equivalent volume of chromophore and TEMP solutions were combined. The resulting solution was then transferred to a quartz capillary tube and promptly examined using EPR spectroscopy. EPR measurements were performed in situ under

photoexcitation in a standard EPR cavity on an X-band Bruker spectrometer equipped with a 365 nm LED (Thorlab), with irradiation times ranging from 0 to 15 min.<sup>116</sup> These EPR assays were carried out at room temperature, with settings including a modulation frequency of 100 kHz, a microwave power of 7 mW, a modulation amplitude of 1 G, a time constant of 20.5 ms, and a single acquisition scan. The temporal change in TEMPO concentration was plotted for both solvents, as illustrated in Fig. S26<sup>†</sup>. The singlet oxygen quantum yield ( $\phi_A$ ) in acetonitrile was determined using reported values for PH. The summarized data are presented in Table 5. The data obtained in MeCN/H<sub>2</sub>O were not subjected to further analysis, as the rate of singlet oxygen generation by **PH** was significantly lower than that of Pd(TPPP) and In(TPPP), despite the expected  $\phi_A$  of 100% for this compound.

### AUTHOR CONTRIBUTIONS

A. K. performed the synthesis of porphyrins, their characterization and catalytic studies. C.M. performed photophysical characterization and writing of the original draft of this article section. L.K. and S.P. proposed to perform EPR studies, carried out these measurements and write of the original draft of this article section. Y. R. was responsible for single crystal X-ray characterization. S.A.S. and C.B. performed electrochemical and spectroelectrochemical characterization, writing of the original draft of this article section and editing of all text. A.V.C. performed DFT calculations. A.B.-L. studied photocatalytic properties. H.N. participated in manuscript editing. A.B.-L. and C.M. were responsible for the project conceptualization, supervision, data analysis, writing and editing of article. S. P. and A.B.-L. was responsible for funding acquisition.

### CONFLICTS OF INTEREST

There are no conflicts to declare.

### ACKNOWLEDGMENTS

The authors thanks Dr. S. Denis-Quanquin for help with NMR spectroscopy and useful discussions. This work was supported by CNRS and ENS de Lyon.

### REFERENCES

1. N. Hoffmann, *Chem. Rev.*, 2008, **108**, 1052–1103.
2. A. A. Ghogare and A. Greer, *Chem. Rev.*, 2016, **116**, 9994–10034.

3. J. M. R. Narayanam and C. R. J. Stephenson, *Chem. Soc. Rev.*, 2011, **40**, 102–113.
4. C. K. Prier, D. A. Rankic and D. W. C. MacMillan, *Chem. Rev.*, 2013, **113**, 5322–5363.
5. D. M. Schultz and T. P. Yoon, *Science*, 2014, **343**, 1239176.
6. N. A. Romero and D. A. Nicewicz, *Chem. Rev.*, 2016, **116**, 10075–10166.
7. T. Koike and M. Akita, *Inorg. Chem. Front.*, 2014, **1**, 562–576.
8. J. D. Bell and J. A. Murphy, *Chem. Soc. Rev.*, 2021, **50**, 9540–9685.
9. G. V. Morozkov, A. S. Abel, M. A. Filatov, S. E. Nefedov, V. A. Roznyatovsky, A. V. Cheprakov, A. Y. Mitrofanov, I. S. Ziankou, A. D. Averin, I. P. Beletskaya, J. Michalak, C. Bucher, L. Bonneviot and A. Bessmertnykh-Lemeune, *Dalton Trans.*, 2022, **51**, 13612–13630.
10. S. DiLuzio, T. U. Connell, V. Mdluli, J. F. Kowalewski and S. Bernhard, *J. Am. Chem. Soc.*, 2022, **144**, 1431–1444.
11. Z. Mahmood, J. He, S. Cai, Z. Yuan, H. Liang, Q. Chen, Y. Huo, B. König and S. Ji, *Chem. – Eur. J.*, 2023, **29**, e202202677.
12. T. Toyao, N. Ueno, K. Miyahara, Y. Matsui, T.-H. Kim, Y. Horiuchi, H. Ikeda and M. Matsuoka, *Chem. Commun.*, 2015, **51**, 16103–16106.
13. K. Rybicka-Jasińska, W. Shan, K. Zawada, K. M. Kadish and D. Gryko, *J. Am. Chem. Soc.*, 2016, **138**, 15451–15458.
14. R. Costa e Silva, L. Oliveira da Silva, A. de Andrade Bartolomeu, T. J. Brocksom and K. T. de Oliveira, *Beilstein J. Org. Chem.*, 2020, **16**, 917–955.
15. S. Kawai, *Yakugaku Zasshi*, 1966, **86**, 1125–1132.
16. J. F. Tanguay, S. L. Suib and R. W. Coughlin, *J. Catal.*, 1989, **117**, 335–347.
17. L. A. Peña, A. M. Chan, L. R. Cohen, K. Hou, B. M. Harvey and P. E. Hoggard, *Photochem. Photobiol.*, 2014, **90**, 760–766.
18. A. Sheldon, *Metalloporphyrins in Catalytic Oxidations*, Marcel Dekker, New York, 1994.
19. N. A. Stephenson and A. T. Bell, *J. Mol. Cat. A: Chem.*, 2007, **272**, 108–117.
20. G. da Silva, S. M. G. Pires, V. L. M. Silva, M. M. Q. Simões, M. G. P. M. S. Neves, S. L. H. Rebelo, A. M. S. Silva and J. A. S. Cavaleiro, *Catal. Commun.*, 2014, **56**, 68–71.
21. C. Maillet, P. Janvier, M. Pipelier, T. Praveen, Y. Andres and B. Bujoli, *Chem. Mater.*, 2001, **13**, 2879–2884.
22. A. Vioux, J. le Bideau, P. H. Mutin and D. Leclercq, *Top. Curr. Chem.*, 2004, **232**, 145–174.
23. A. D. G. Firmino, F. Figueira, J. P. C. Tomé, F. A. A. Paz and J. Rocha, *Coord. Chem. Rev.*, 2018, **355**, 133–149.
24. P. Kubát, K. Lang and P. Anzenbacher, *Biochim. Biophys. Acta*, 2004, **1670**, 40–48.
25. G. V. Morozkov, A. S. Abel, K. A. Lyssenko, V. A. Roznyatovsky, A. D. Averin, I. P. Beletskaya and A. Bessmertnykh-Lemeune, *Dalton Trans.*, 2024, **53**, 535–551.
26. N. Venkatramaiah, C. F. Pereira, R. F. Mendes, F. A. A. Paz and J. P. C. Tomé, *Anal. Chem.*, 2015, **87**, 4515–4522.
27. T. Rhauderwiek, K. Wolkersdörfer, S. Øien-Ødegaard, K.-P. Lillerud, M. Wark and N. Stock, *Chem. Commun.*, 2018, **54**, 389–392.
28. M. M. Ayhan, C. Bayraktar, K. B. Yu, G. Hanna, A. O. Yazaydin, Y. Zorlu and G. Yücesan, *Chem. – Eur. J.*, 2020, **26**, 14813–14816.
29. M.-F. Qin, C.-Y. Wang, S.-S. Bao and L.-M. Zheng, *Chem. Commun.*, 2022, **58**, 8372–8375.
30. K. M. Kadish, P. Chen, Y. Y. Enakieva, S. E. Nefedov, Y. G. Gorbunova, A. Y. Tsivadze, A. Bessmertnykh-Lemeune, C. Stern and R. Guillard, *J. Electroanal. Chem.*, 2011, **656**, 61–71.
31. R. Kumar, P. Yadav, A. Kumar and M. Sankar, *Chem. Lett.*, 2015, **44**, 914–916.

32. E. B. Fleischer and T. S. Srivastava, *Inorg. Chim. Acta*, 1971, **5**, 151–154.
33. D. A. Summerville, R. D. Jones, B. M. Hoffman and F. Basolo, *J. Am. Chem. Soc.*, 1977, **99**, 8195–8202.
34. P. Tholen, C. A. Peeples, M. M. Ayhan, L. Wagner, H. Thomas, P. Imbrasas, Y. Zorlu, C. Baretzky, S. Reineke, G. Hanna and G. Yücesan, *Small*, 2022, **18**, 2204578.
35. E. B. Fleischer, C. K. Miller and L. E. Webb, *J. Am. Chem. Soc.*, 1964, **86**, 2342–2347.
36. A. J. Golder, K. B. Nolan, D. C. Povey and L. R. Milgrom, *Acta Crystallogr., Sect. C: Cryst. Struct. Commun.*, 1988, **44**, 1916–1921.
37. W.-T. Chen, R.-H. Hu, Z.-G. Luo and H.-L. Chen, *Asian J. Chem.*, 2015, **27**, 775–776.
38. K. A. Lyssenko, G. V. Grintselev-Knyazev and M. Y. Antipin, *Mendeleev Commun.*, 2002, **12**, 128–130.
39. E. Y. Tupikina, M. Bodensteiner, P. M. Tolstoy, G. S. Denisov and I. G. Shenderovich, *J. Phys. Chem. C*, 2018, **122**, 1711–1720.
40. S. Lie, T. Maris and J. D. Wuest, *Cryst. Growth Des.*, 2014, **14**, 3658–3666.
41. C. Heering, B. Nateghi and C. Janiak, *Crystals*, 2016, **6**, 22.
42. C. F. Macrae, I. J. Bruno, J. A. Chisholm, P. R. Edgington, P. McCabe, E. Pidcock, L. Rodriguez-Monge, R. Taylor, J. van de Streek and P. A. Wood, *J. Appl. Crystallogr.*, 2008, **41**, 466–470.
43. A. A. Sinelshchikova, Y. Y. Enakieva, M. S. Grigoriev and Y. G. Gorbunova, *J. Struct. Chem.*, 2022, **63**, 874–884.
44. I. Goldberg, *Chem. Commun.*, 2005, 1243–1254.
45. P. Tholen, C. A. Peeples, R. Schaper, C. Bayraktar, T. S. Erkal, M. M. Ayhan, B. Çoşut, J. Beckmann, A. O. Yazaydin, M. Wark, G. Hanna, Y. Zorlu and G. Yücesan, *Nat. Commun.*, 2020, **11**, 3180.
46. H. Zhao, Z. Zhou, X. Feng, C. Liu, H. Wu, W. Zhou and H. Wang, *Nano Research*, 2023, **16**, 8809–8816.
47. A. A. Sinelshchikova, S. E. Nefedov, Y. Y. Enakieva, Y. G. Gorbunova, A. Y. Tsivadze, K. M. Kadish, P. Chen, A. Bessmertnykh-Lemeune, C. Stern and R. Guilard, *Inorg. Chem.*, 2013, **52**, 999–1008.
48. Y. Fang, Y. G. Gorbunova, P. Chen, X. Jiang, M. Manowong, A. A. Sinelshchikova, Y. Y. Enakieva, A. G. Martynov, A. Y. Tsivadze, A. Bessmertnykh-Lemeune, C. Stern, R. Guilard and K. M. Kadish, *Inorg. Chem.*, 2015, **54**, 3501–3512.
49. K. M. Kadish, E. Van Caemelbecke and G. Royal, in *The Porphyrin Handbook*, eds. K. M. Kadish, K. M. Smith and R. Guilard, Academic Press, San Diego, 2000, vol. 8, pp. 1–114.
50. X. Ke, R. Kumar, M. Sankar and K. M. Kadish, *Inorg. Chem.*, 2018, **57**, 1490–1503.
51. K. M. Kadish, J. L. Cornillon, P. Cocolios, A. Tabard and R. Guilard, *Inorg. Chem.*, 1985, **24**, 3645–3649.
52. V. V. Pavlishchuk and A. W. Addison, *Inorg. Chim. Acta*, 2000, **298**, 97–102.
53. C. Inisan, J.-Y. Saillard, R. Guilard, A. Tabard and Y. Le Mest, *New J. Chem.*, 1998, **22**, 823–830.
54. R. Feng, Z. Ou, Z. Xue, Y. Fang, Y. Song and K. M. Kadish, *RSC Adv.*, 2015, **5**, 96769–96776.
55. C. H. Devillers, A. Milet, J.-C. Moutet, J. Pécaut, G. Royal, E. Saint-Aman and C. Bucher, *Dalton Trans.*, 2013, **42**, 1196–1209.
56. K. M. Kadish, G. Royal, E. Van Caemelbecke and L. Gueletti, in *The Porphyrin Handbook*, eds. K. M. Kadish, K. M. Smith and R. Guilard, Academic Press, San Diego, CA, 2000, vol. 9, pp. 1–219.
57. K. M. Kadish and E. Van Caemelbecke, *J. Solid State Electrochem.*, 2003, **7**, 254–258.
58. J. H. Furhop, K. M. Kadish and D. G. Davis, *J. Am. Chem. Soc.*, 1973, **95**, 5140–5147.

59. J. G. Lanese and G. S. Wilson, *J. Electrochem. Soc.*, 1972, **119**, 1039.
60. G. S. Wilson and G. Peychal-Heiling, *Anal. Chem.*, 1971, **43**, 545–550.
61. W.-P. To, Y. Liu, T.-C. Lau and C.-M. Che, *Chem. – Eur. J.*, 2013, **19**, 5654–5664.
62. R. H. Felton and H. Linschitz, *J. Am. Chem. Soc.*, 1966, **88**, 1113–1116.
63. L. A. Truxillo and D. G. Davis, *Anal. Chem.*, 1975, **47**, 2260–2267.
64. K. M. Kadish and D. G. Davis, *Ann. N. Y. Acad. Sci.*, 1973, **206**, 495–503.
65. F. D'Souza and V. Krishnan, *J. Chem. Soc., Dalton Trans.*, 1992, 2873–2876.
66. M. Taniguchi, J. S. Lindsey, D. F. Bocian and D. Holten, *J. Photochem. Photobiol., C*, 2021, **46**, 100401.
67. H. L. Kee, J. Bhaumik, J. R. Diers, P. Mroz, M. R. Hamblin, D. F. Bocian, J. S. Lindsey and D. Holten, *J. Photochem. Photobiol., A*, 2008, **200**, 346–355.
68. D. S. Sharada, A. Z. Muresan, K. Muthukumaran and J. S. Lindsey, *J. Org. Chem.*, 2005, **70**, 3500–3510.
69. O. Ohno, Y. Kaizu and H. Kobayashi, *J. Chem. Phys.*, 1985, **82**, 1779–1787.
70. A. R. d. Silva, A. C. Pelegrino, A. C. Tedesco and R. A. Jorge, *J. Braz. Chem. Soc.*, 2008, **19**, 491–501.
71. Y. Belghith, A. Mansour, J. Daran and H. Nasri, *Open J. Inorg. Chem.*, 2012, **2**, 81–87.
72. Y. Kurabayashi, K. Kikuchi, H. Kokubun, Y. Kaizu and H. Kobayashi, *J. Phys. Chem.*, 1984, **88**, 1308–1310.
73. M. Gouterman, *J. Mol. Spectrosc.*, 1961, **6**, 138–163.
74. R. Giovannetti, in *Macro To Nano Spectroscopy*, ed. J. Uddin, InTech, Rijeka, Croatia, 2012, pp. 87–108.
75. E. Y. Kaigorodova, G. M. Mamardashvili, O. R. Simonova, N. V. Chizhova and N. Z. Mamardashvili, *J. Coord. Chem.*, 2021, **74**, 2443–2462.
76. M. Ghosh and S. Sinha, *Spectrochim. Acta, Part A*, 2015, **150**, 959–965.
77. R. Teixeira, V. V. Serra, D. Botequim, P. M. R. Paulo, S. M. Andrade and S. M. B. Costa, *Molecules*, 2021, **26**, 4246.
78. K. A. Stingl and S. B. Tsogoeva, *Tetrahedron: Asymmetry*, 2010, **21**, 1055–1074.
79. Y. Liu, A. J. Howarth, J. T. Hupp and O. K. Farha, *Angew. Chem., Int. Ed.*, 2015, **54**, 9001–9005.
80. J. Han, V. A. Soloshonok, K. D. Klika, J. Drabowicz and A. Wzorek, *Chem. Soc. Rev.*, 2018, **47**, 1307–1350.
81. H. Yu, Z. Li and C. Bolm, *Angew. Chem., Int. Ed.*, 2018, **57**, 324–327.
82. M. Ahmadian and M. Anbia, *Energy Fuels*, 2021, **35**, 10347–10373.
83. E. Baciocchi, C. Crescenzi and O. Lanzalunga, *Tetrahedron*, 1997, **53**, 4469–4478.
84. E. Baciocchi, T. Del Giacco, O. Lanzalunga, P. Mencarelli and B. Procacci, *J. Org. Chem.*, 2008, **73**, 5675–5682.
85. R. V. Kupwade, *J. Chem. Rev.*, 2019, **1**, 99–113.
86. S. Matavos-Aramyan, S. Soukhakian and M. H. Jazebizadeh, *Phosphorus, Sulfur Silicon Relat. Elem.*, 2020, **195**, 181–193.
87. S. Caron, R. W. Dugger, S. G. Ruggeri, J. A. Ragan and D. H. B. Ripin, *Chem. Rev.*, 2006, **106**, 2943–2989.
88. J. C. Barona-Castaño, C. C. Carmona-Vargas, T. J. Brocksom and K. T. De Oliveira, *Molecules*, 2016, **21**, 310.
89. E. Skolia, P. L. Gkizis and C. G. Kokotos, *ChemPlusChem*, 2022, **87**, e202200008.
90. T. Hikita, K. Tamaru, A. Yamagishi and T. Iwamoto, *Inorg. Chem.*, 1989, **28**, 2221–2223.
91. E. Baciocchi, T. D. Giacco, F. Elisei, M. F. Gerini, M. Guerra, A. Lapi and P. Liberali, *J. Am. Chem. Soc.*, 2003, **125**, 16444–16454.

92. S. M. Bonesi, I. Manet, M. Freccero, M. Fagnoni and A. Albini, *Chem. – Eur. J.*, 2006, **12**, 4844–4857.
93. E. L. Clennan, *Acc. Chem. Res.*, 2001, **34**, 875–884.
94. A. G. Mojarrad and S. Zakavi, *Catal. Sci. Technol.*, 2018, **8**, 768–781.
95. C. Liu, K. Liu, C. Wang, H. Liu, H. Wang, H. Su, X. Li, B. Chen and J. Jiang, *Nat. Commun.*, 2020, **11**, 1047.
96. I. A. Abdulaeva, *PhD thesis, Université de Bourgogne and Lomonosov Moscow state university, Dijon, France and Moscow, Russia*, 2017.
97. D. A. Polivanovskaia, I. A. Abdulaeva, K. P. Birin, Y. G. Gorbunova and A. Y. Tsivadze, *J. Catal.*, 2022, **413**, 342–352.
98. S. Ribeiro, A. C. Serra and A. M. d. A. Rocha Gonsalves, *ChemCatChem*, 2013, **5**, 134–137.
99. C. Yingzhi, H. Zheng-Hong and W. Lu-Ning, in *Phthalocyanines and Some Current Applications*, ed. Y. Yusuf, IntechOpen, Rijeka, 2017, p. Ch. 6.
100. J. Jiang, R. Luo, X. Zhou, Y. Chen and H. Ji, *Adv. Synth. Catal.*, 2018, **360**, 4402–4411.
101. R. Nasrollahi, A. Heydari-turkmani and S. Zakavi, *Catal. Sci. Technol.*, 2019, **9**, 1260–1272.
102. M.-F. Qin, Q.-Q. Mu, S.-S. Bao, X. Liang, Y. Peng and L.-M. Zheng, *ACS Appl. Energy Mater.*, 2021, **4**, 4319–4326.
103. K. Feng, H. Hao, F. Huang, X. Lang and C. Wang, *Mater. Chem. Front.*, 2021, **5**, 2255–2260.
104. G. Lu, F. Chu, X. Huang, Y. Li, K. Liang and G. Wang, *Coord. Chem. Rev.*, 2022, **450**, 214240.
105. I. A. Abdulaeva, K. P. Birin, R. Chassagnon and A. Bessmertnykh-Lemeune, *Catalysts*, 2023, **13**, 402.
106. X. Gu, X. Li, Y. Chai, Q. Yang, P. Li and Y. Yao, *Green. Chem.*, 2013, **15**, 357–361.
107. L. Wang, J. Cao, J.-w. Wang, Q. Chen, A.-j. Cui and M.-y. He, *RSC Adv.*, 2014, **4**, 14786–14790-
108. R. Cibulka, *Eur. J. Org. Chem.*, 2015, **2015**, 915–932.
109. C. Dang, L. Zhu, H. Guo, H. Xia, J. Zhao and B. Dick, *ACS Sustainable Chem. Eng.*, 2018, **6**, 15254–15263.
110. X. Liang, Z. Guo, H. Wei, X. Liu, H. Lv and H. Xing, *Chem. Commun.*, 2018, **54**, 13002–13005.
111. C. F. Pereira, Y. Liu, A. Howarth, F. Figueira, J. Rocha, J. T. Hupp, O. K. Farha, J. P. C. Tomé and F. A. Almeida Paz, *ACS Appl. Nano Mater.*, 2019, **2**, 465–469.
112. T. Neveselý, E. Svobodová, J. Chudoba, M. Sikorski and R. Cibulka, *Adv. Synth. Catal.*, 2016, **358**, 1654–1663.
113. M. C. DeRosa and R. J. Crutchley, *Coord. Chem. Rev.*, 2002, **233–234**, 351–371.
114. R. Schmidt, C. Tanielian, R. Dunsbach and C. Wolff, *J. Photochem. Photobiol., A*, 1994, **79**, 11–17.
115. F. Wilkinson, W. P. Helman and A. B. Ross, *J. Phys. Chem. Ref. Data*, 1993, **22**, 113–262.
116. C. Mendoza, A. Désert, L. Khrouz, C. A. Páez, S. Parola and B. Heinrichs, *Environ. Sci. Pollut. Res.*, 2021, **28**, 25124–25129.
117. W. He, Y. Liu, W. G. Wamer and J.-J. Yin, *J. Food Drug Anal.*, 2014, **22**, 49–63.
118. G. Nardi, I. Manet, S. Monti, M. A. Miranda and V. Lhiaubet-Vallet, *Free Radical Biol. Med.*, 2014, **77**, 64–70.
119. H. Hennig, J. Behling, R. Meusinger and L. Weber, *Chem. Ber.*, 1995, **128**, 229–234.
120. I. Kikaš, O. Horváth and I. Škorić, *Tetrahedron Lett.*, 2011, **52**, 6255–6259.

121. M. Mlakić, A. Šalić, M. Bačić, B. Zelić, I. Šagud, O. Horváth and I. Škorić, *Catalysts*, 2021, **11**, 395.
122. A. A. Granovsky, Firefly version 8, <http://classic.chem.msu.su/gran/firefly/index.html> (accessed 20 january, 2024).
123. M. Dolg, H. Stoll, H. Preuss and R. M. Pitzer, *J. Phys. Chem.* 1993, **97**, 5852–5859.
124. G. Sheldrick, *Acta Crystallogr., Sect. C: Struct. Chem.*, 2015, **71**, 3–8.
125. G. Sheldrick, *Acta Crystallogr., Sect. A: Found. Adv.*, 2015, **71**, 3–8.
126. O. V. Dolomanov, L. J. Bourhis, R. J. Gildea, J. A. K. Howard and H. Puschmann, *J. Appl. Crystallogr.*, 2009, **42**, 339–341.
127. H. Ishida, S. Tobita, Y. Hasegawa, R. Katoh and K. Nozaki, *Coord. Chem. Rev.*, 2010, **254**, 2449–2458.
128. M. Levitus, *Methods Appl. Fluoresc.*, 2020, **8**, 033001